UNIVERSITÀ DEGLI STUDI DI PADOVA

DIPARTIMENTO DI BIOLOGIA

Corso di Laurea in Biologia Molecolare

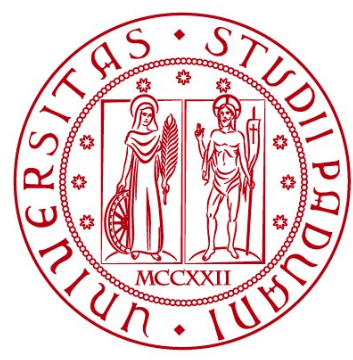

ELABORATO DI LAUREA

Il metabolismo della serina nel trattamento del cancro ovarico

Tutor: Prof. Luigi Leanza
Dipartimento di Biologia

Laureanda: Mariasole Sturaro
Matricola: 1237859

ANNO ACCADEMICO 2022/2023

INDICE

ABSTRACT 3

1. INTRODUZIONE 5

1.1 Metabolismo delle cellule tumorali 5

1.2 Metabolismo della serina 5

1.3 Cancro ovarico 7

1.4 Trattamenti per il cancro epiteliale ovarico 8

2. MATERIALI E METODI 11

2.1 Western blot 11

2.2 Gascromatografia e cromatografia liquida associate a spettrometria di massa (GC-MS e LC-MS) 11

2.2.1 Tecniche cromatografiche 11

2.2.2 Spettrometria di massa 12

2.3 RNA-sequencing (RNA-seq) 12

2.3.1 Next Generation Sequencing – Illumina 13

2.4 Modelli impiegati nello studio 14

2.4.1 Modelli in vitro: colture cellulari 14

2.4.2 Modelli in vivo: topi PDX (Patient Derived Xenografts) 14

2.4.3 Modelli ex vivo: organoidi 14

3. RISULTATI 15

3.1 Diminuzione dell'espressione di PHGDH e ridotta attività biosintetica della serina nelle pazienti con recidiva resistente alla chemioterapia a base di platino 15

3.2 Le cellule resistenti sono auxotrofiche per la serina 17

3.3 Le cellule resistenti al platino riconfigurano le vie di rigenerazione del NAD+ 18

3.4 Le cellule resistenti al platino aumentano l'attività dei PARP e l'inibizione di questi enzimi ri-sensibilizza le cellule al carboplatino 19

4. DISCUSSIONE 21

BIBLIOGRAFIA 23

APPENDICE 25

ABSTRACT

La resistenza alla chemioterapia a base di platino rappresenta un ostacolo importante nel trattamento di molti tumori. In particolare nel tumore ovarico, molte pazienti sperimentano diversi cicli di risposta-recidiva, fino ad arrivare a sviluppare la resistenza al trattamento, che diventa una delle principali cause di prognosi sfavorevole.

La biosintesi della serina è stata in generale correlata alla crescita di diversi tipi di tumore, tuttavia, il suo ruolo nello sviluppo della resistenza al platino nel cancro ovarico non è stato ancora studiato.

L'articolo in esame mostra che in un sottogruppo di tumori ovarici resistenti, a seguito di chemioterapia a base di platino, si assiste alla diminuzione dell'espressione della fosfoglicerato deidrogenasi (PHGDH), l'enzima principale coinvolto nella via di biosintesi della serina. Nello specifico è emerso che l'entità della riduzione dei livelli di PHGDH correla con una prognosi peggiore. Lo studio mette inoltre in evidenza che il riarrangiamento della biosintesi della serina è accompagnato da un fenotipo che risparmia NAD+, il coenzima da cui dipende l'attività di PHGDH, e che sostiene l'attività degli enzimi PARP, coinvolti nella riparazione dei danni al DNA, suggerendo così la possibilità di nuove terapie.

1. INTRODUZIONE

1.1 Metabolismo delle cellule tumorali

È noto che le cellule sane generano l'energia necessaria per i processi cellulari, sottoforma di adenosina trifosfato (ATP), grazie alla respirazione cellulare, processo che avviene in presenza di ossigeno e vede al suo interno diverse tappe, tra cui la glicolisi e la fosforilazione ossidativa. Le cellule tumorali invece, anche in presenza di ossigeno e di mitocondri completamente funzionanti, prediligono la glicolisi aerobica seguita dalla fermentazione del glucosio in lattato. Questa alterazione del metabolismo prende il nome di "effetto Warburg" (Liberti & Locasale, 2016). È un fenomeno che potrebbe sembrare svantaggioso in quanto la glicolisi aerobica non porta ad un'elevata produzione di ATP, come invece avviene con la respirazione cellulare. Una delle ipotesi, è che ci sia un vantaggio dal punto di vista metabolico: il metabolismo delle cellule tumorali, infatti, subisce degli adattamenti che portano ad un più facile assorbimento dei nutrienti (nucleotidi, amminoacidi e lipidi) necessari per la proliferazione (Amelio et al., 2014). Una caratteristica di questo adattamento metabolico è l'aumento del consumo di glucosio che viene poi utilizzato anche come fonte di carbonio per i processi utili alla proliferazione cellulare. Questa condizione porta ad un eccesso di carbonio che viene indirizzato nelle vie metaboliche che derivano dal flusso glicolitico. Un esempio è la biosintesi della serina a partire dal glucosio, mediata dall'enzima fosfoglicerato deidrogenasi (PHGDH). Questa via metabolica è una delle più studiate ed è stata collegata allo sviluppo e alla progressione di differenti tipi di cancro. Si può notare che in questo contesto è particolarmente coinvolto il metabolismo degli amminoacidi. Alcuni di questi, infatti, come la serina, ma anche la glicina (che deriva dalla serina), forniscono i precursori per la sintesi di nutrienti cruciali per la crescita delle cellule tumorali. Inoltre, la sovra-espressione dei trasportatori del glucosio nelle cellule tumorali garantisce loro una larga abbondanza del nutriente a discapito delle cellule adiacenti.

1.2 Metabolismo della serina

La serina è un amminoacido non essenziale polare, la cui disponibilità è cruciale per molti processi cellulari. La biosintesi della serina è una via metabolica strettamente connessa alla glicolisi, infatti, essa viene prodotta in tre fasi successive a partire dal 3-fosfoglicerato, un intermedio glicolitico. Il 3-fosfoglicerato viene convertito prima in 3-fosfoidrossipiruvato dall'enzima PHGDH, poi in 3-fosfoserina dall'enzima fosfoserina aminotransferasi (PSAT1), e infine in serina dall'enzima fosfoserina fosfatasi (PSPH) [Figura 1].
Analizzando il metabolismo della serina nelle cellule tumorali, è stato osservato che c'è una sovra-regolazione di questo processo. Queste cellule utilizzano PHGDH e nicotinammide adenina dinucleotide nella forma ossidata (NAD+) per ossidare circa il 10% del 3-fosofoglicerato.

In particolare, in alcuni tipi di tumori (es. carcinoma mammario triplo negativo e melanoma) è stata osservata una sovra-espressione di PHGDH, portando quindi a convalidare l'ipotesi che la serina sia un amminoacido molto richiesto e indispensabile per le cellule tumorali.

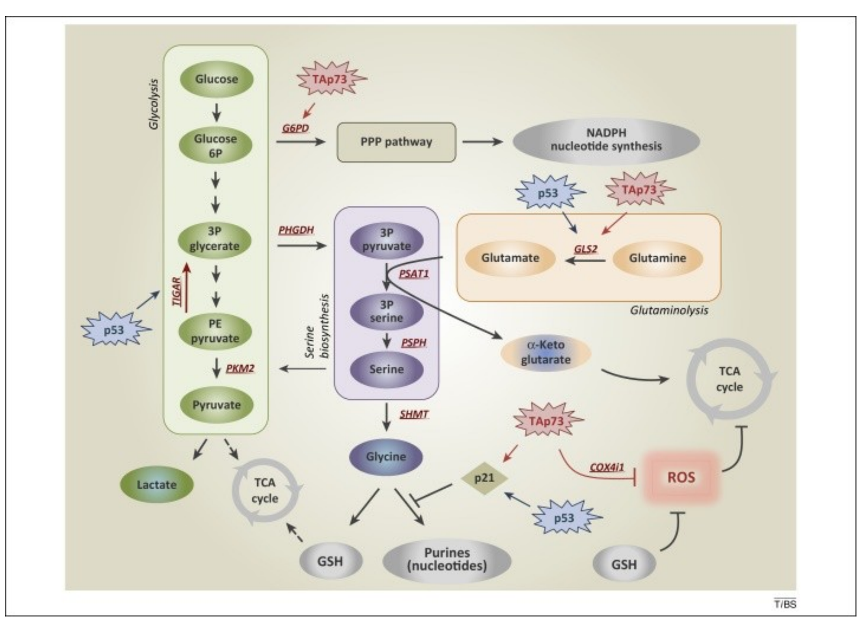

***Figura 1**: A sinistra dell'immagine è rappresentata la biosintesi de novo della serina a partire dall'intermedio glicolitico 3-fosfoglicerato, mediata dalla PHGDH. (Amelio et al., 2014)*

La serina è un importante donatore di C1 al ciclo dei folati, si parla di "*one-carbon metabolism*". Quest'unità di carbonio è essenziale perché entrando nel ciclo dei folati porta alla sintesi dei nucleotidi e alla metilazione e generazione di nicotinammide adenina dinucleotide fosfato (NADPH), che rappresenta il potere antiossidante della cellula. Si tratta di processi che sostenendo la replicazione cellulare favoriscono la proliferazione del tumore. Essendo quindi la serina una delle principali fonti di C1, si è visto che carenze di questo amminoacido o l'inibizione della sua sintesi hanno un effetto diretto sulle cellule tumorali (Yang & Vousden, 2016). Per sviluppare strategie antitumorali, in passato si è lavorato sul "*one-carbon metabolism*", e fino ad oggi, sono stati progettati ed impiegati diversi chemioterapici che vanno ad agire su bersagli presenti all'interno del ciclo dei folati. Successivamente sono stati individuati anche altri possibili "*target*" che coinvolgono ad esempio la biosintesi della serina, della glicina e la dieta; si tratta di studi tutt'ora in fase di sviluppo, potenzialmente molto interessanti in quanto potrebbero portare a nuovi approcci terapeutici [Figura 2] (Newman & Maddocks, 2017).

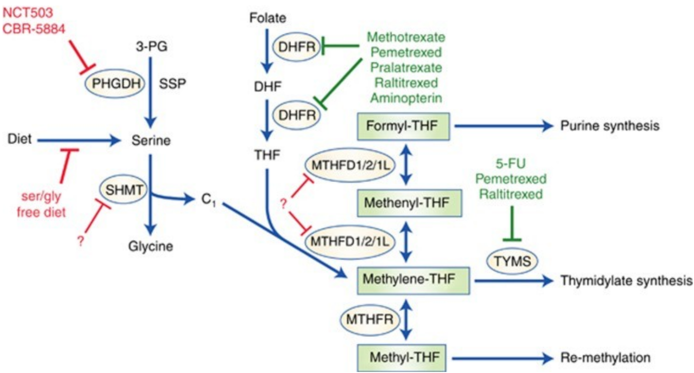

***Figura 2**: Visione d'insieme del "one-carbon metabolism". In verde sono evidenziati i chemioterapici già in utilizzo (con i rispettivi targets), in rosso invece sono evidenziati altri possibili targets ancora oggetto di studio. (Newman & Maddocks, 2017)*

Nella via della biosintesi della serina, come accennato in precedenza, la PHGDH ha bisogno della presenza del coenzima NAD+. Essendo la produzione di purine dipendente dal "*one-carbon metabolism*" che, a sua volta, è connesso alla disponibilità di serina, se non sono presenti adeguati livelli di NAD+ le cellule tumorali non riescono a mantenere la loro massima proliferazione.

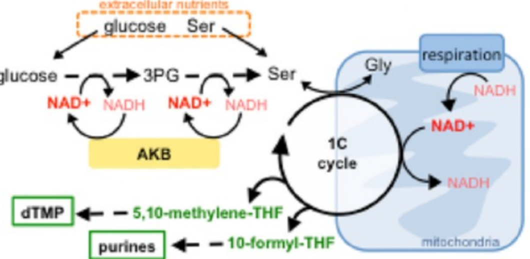

***Figura 3**: Come la presenza del coenzima NAD+ influisce sul percorso di biosintesi della serina, sul ciclo dell'acido folico e quindi infine sulla produzione delle basi puriniche. Inoltre, viene evidenziato il ripristino sempre del NAD+ a partire dal NADH attraverso respirazione cellulare e riduzione dell'AKB. (Diehl et al., 2019)*

In questo contesto il NAD+ può essere rigenerato a partire dal NADH (la forma ridotta) attraverso la respirazione mitocondriale o altrimenti dalla riduzione dell'α-chetobutirrato (AKB) [Figura 3]. Le cellule tumorali, inoltre, assorbono anche dall'ambiente esterno grandi quantità di serina (sia che la disponibilità di serina endogena sia compromessa o meno), per cui anche la serina esogena è necessaria per arrivare ad avere la massima proliferazione cellulare (Diehl et al., 2019).

1.3 Cancro ovarico

Il cancro ovarico ha origine nei tessuti delle ovaie, due organi di circa tre centimetri di diametro connessi all'utero tramite le tube di Falloppio, con la funzione di produrre gli ormoni sessuali (estrogeni e progesterone) e gli oociti. I tre tipi di cellule che costituiscono le ovaie sono: epiteliali, germinali e stromali; e in base a quali cellule vengono coinvolte si possono sviluppare rispettivamente tre diverse tipologie di cancro ovarico: epiteliale, germinale o stromale.
Il cancro epiteliale ovarico, in particolare, origina dalle cellule epiteliali che rivestono la superficie delle ovaie e ha una predisposizione genetica nel 15% delle donne affette, in questo senso le mutazioni ereditarie nei geni BRCA1 e BRCA2 (geni di suscettibilità anche del cancro al seno) sono un importante fattore di rischio. Altri fattori di rischio sono ad esempio un periodo ovulatorio di lunga

durata (quindi un menarca precoce e/o una menopausa tardiva) e l'assenza di gravidanze.
Il cancro epiteliale ovarico è composto da diversi sottotipi, che si possono distinguere per caratteristiche istologiche differenti, e tra questi il più rappresentato è il carcinoma ovarico sieroso di alto grado o "*high-grade serous carcinoma*" (HGSC). Esso si sviluppa dall'epitelio ovarico fino all'epitelio distale della tuba di Falloppio, rappresenta circa il 70% di tutte le tipologie di cancro ovarico ed è causa di molti decessi. Oltre al cancro ovarico di origine epiteliale, che costituisce più del 90% delle neoplasie ovariche maligne, come detto in precedenza possono presentarsi altre due tipologie di cancro ovarico: germinale, che deriva dalle cellule da cui originano gli oociti (circa il 5% delle neoplasie ovariche maligne), e stromale, che deriva dal tessuto strutturale dell'ovaio che produce gli ormoni sessuali (circa l'1% di tutti i tumori ovarici) (Stewart et al., 2019).

1.4 Trattamenti per il cancro epiteliale ovarico

Il cancro epiteliale ovarico è uno dei tumori ginecologici più letali e ha circa il 45% di sopravvivenza a 5 anni dalla diagnosi. Uno dei motivi per cui ha una letalità così alta è che viene diagnosticato quando è già ad uno stadio avanzato (circa il 75% dei casi) a causa della sua natura asintomatica. Dato che gli screening si sono mostrati inefficaci, si stanno sviluppando nuovi approcci per una diagnosi precoce e per la prevenzione che andrebbero a sfruttare la genomica molecolare.
Per questa tipologia di cancro i trattamenti previsti sono la *Primary Debulking Surgery* (PDS) (o rimozione chirurgica) seguita dalla terapia adiuvante, ovvero la chemioterapia, o altrimenti, un'altra linea d'azione è la chemioterapia neoadiuvante (NACT) seguita da *Interval debulking Surgery* (IDS) (o chirurgia d'intervallo, una tipologia di citoriduzione). La IDS viene scelta rispetto alla PDS nel caso in cui quest'ultima non possa essere eseguita. I motivi di ciò possono essere vari, ad esempio se il tumore è già molto esteso o per le condizioni cliniche della paziente. Da studi clinici è stato valutato che non c'è una differenza sostanziale nell'utilizzo della PDS o dell'IDS (Lheureux et al., 2019).
La maggior parte degli studi sulle terapie indicate per il cancro epiteliale ovarico sono state fatte sull'HGSC, per cui la terapia di prima linea è stata stabilita soprattutto a partire da questo sottogruppo.
In particolare, la chemioterapia che viene eseguita a seguito di PDS, come adiuvante, è una chemioterapia a base di platino (cisplatino o carboplatino) e taxani (paclitaxel). Il cisplatino e il carboplatino sono agenti chemioterapici che hanno la capacità di inibire la sintesi di DNA e quindi bloccare la proliferazione delle cellule tumorali. Riescono a legarsi al DNA attraverso la formazione di legami crociati tra filamenti complementari, interferendo così con il ciclo cellulare. Il carboplatino è un analogo di seconda generazione del cisplatino con la differenza risulta meglio tollerato. Il paclitaxel è un agente chemioterapico che

invece va ad inibire la mitosi (la divisione nucleare) e quindi anche in questo caso la proliferazione.
Un altro aiuto nel trattamento del cancro ovarico sono degli agenti mirati, un esempio sono gli inibitori delle poli ADP-ribosio polimerasi (PARPs). I PARPs sono una famiglia di proteine che hanno la funzione di riparare rotture a singolo filamento del DNA. Si è visto che i cancri ovarici con mutazioni nei geni BRCA1 e BRAC2 sono sensibili agli inibitori dei PARP in quanto questi ultimi portano all'accumulo di rotture del DNA che non vengono riparate causando la morte delle cellule tumorali; questo fenomeno viene chiamato "*synthetic lethality*" (Lheureux et al., 2019).
Dagli studi retrospettivi si è visto che la risposta iniziale alla chemioterapia è molto buona, si osserva infatti nell'80% circa delle pazienti, purtroppo però molte di queste con il tempo vanno in contro a recidive. Uno dei maggiori problemi nel caso dell'utilizzo della chemioterapia a base di platino è che le pazienti sviluppano una resistenza al platino, che non consente più l'impiego del farmaco. Queste pazienti, essendo la recidiva solitamente incurabile, vengono trattate semplicemente tenendo sotto controllo la malattia ed impiegando cure palliative.

2. MATERIALI E METODI

2.1 Western blot

Questa tecnica, utilizzata nella maggior parte degli esperimenti svolti nello studio, permette di valutare e confrontare in condizioni diverse la quantità di varie proteine. In particolare, è stata ad esempio utilizzata per valutare i livelli degli enzimi coinvolti nel processo di biosintesi della serina, soprattutto PHGDH, e i livelli degli enzimi PARP.

Il Western blot, o immunoblot, è una tecnica che si basa sull'utilizzo di anticorpi per identificare e quantificare una determinata proteina presente in un estratto, separata dalle altre proteine in base al peso molecolare, mediante gel elettroforesi, e successivamente trasferita su membrana immobilizzante, mantenendo la separazione ottenuta dal gel. Tra i vantaggi di questa tecnica c'è un'elevata specificità in quanto unisce due tecniche, l'elettroforesi e l'interazione antigene-anticorpo, che consentono elevata risoluzione ed amplificazione del segnale.
Le proteine si separano in base alla loro dimensione a partire dal *running gel*. Successivamente si va a trasferire le proteine dal gel alla membrana ("*blotting*") e a saturare i siti specifici della membrana stessa ("*blocking*"). In seguito, si fa l'incubazione con l'anticorpo primario specifico per l'antigene e infine con l'anticorpo secondario, dalle cui caratteristiche dipende la metodica di rilevazione del segnale ("*detection*").

2.2 Gascromatografia e cromatografia liquida associate a spettrometria di massa (GC-MS e LC-MS)

La cromatografia è una tecnica di separazione di molecole sulla base della loro distribuzione in due diverse fasi: la fase stazionaria (fissa) e la fase mobile (che passa attraverso la fase stazionaria). Si tratta di una tecnica di tipo qualitativo, quantitativo e preparativo (in quanto le molecole purificate possono essere poi utilizzate per ulteriori analisi). Questa tecnica viene poi associata alla spettrometria di massa (MS) con lo scopo di misurare la massa delle molecole.

2.2.1 Tecniche cromatografiche

Esistono due tipologie di cromatografia: gas (GC) e liquida (LC).
Questa tecnica prevede l'utilizzo di colonne cromatografiche, composte da un supporto solido (inerte), dalla fase stazionaria, legata covalentemente al supporto solido, e dalla fase mobile, detta anche eluente (liquida o gas). In queste colonne verrà caricato il campione eterogeneo da separare nelle sue componenti opportunamente preparato in fase gassosa o liquida. In ordine, i passaggi di questa metodica prevedono prima il caricamento della fase stazionaria nella colonna e poi l'aggiunta della miscela delle molecole da separare. Una volta che tra queste è avvenuta l'interazione, si aggiunge gradualmente la fase mobile.

Nella colonna si crea a questo punto un equilibrio tra le due fasi secondo una costante di ripartizione, che definisce l'affinità di una sostanza per la fase stazionaria rispetto a quella mobile. Sulla base di questa affinità, le varie componenti della miscela usciranno dalla colonna con tempistiche diverse. In questo senso, se due proteine hanno la stessa costante di ripartizione (ovvero co-eluiscono) è inefficace tentare di separarle mediante la stessa colonna cromatografica. Il legame che c'è tra la fase stazionaria e il supporto solido è di tipo covalente, invece, il legame delle macromolecole alla fase stazionaria è di tipo non covalente, e quindi reversibile. In questo modo si possono recuperare le molecole di interesse con un opportuno diluente.

2.2.2 Spettrometria di massa

La spettrometria di massa (MS) è una tecnica analitica che consente l'identificazione e l'analisi quantitativa di una molecola dalla sua massa, spesso impiegata assieme ad altre tecniche. Serve a misurare con elevata sensibilità la massa delle molecole, che per la misurazione devono essere ionizzate (cariche).
La MS affianca le tecniche separative, infatti in questo studio si aggiunge sempre alla GC e alla LC. Le molecole per questa metodica devono quindi essere trasformate in ioni, poiché lo strumento che si utilizza, lo spettrometro di massa, va di fatto a misurare il rapporto massa/carica (m/z). Questo rapporto viene poi utilizzato per costruite un grafico che vede in ascissa il rapporto massa/carica e in ordinata i valori di abbondanza relativa degli ioni. Il grafico viene chiamato spettro di massa. Ci sono due caratteristiche fondamentali dello spettrometro di massa: l'accuratezza e la risoluzione. Con accuratezza si intende quanto il valore misurato sperimentalmente si avvicina al valore reale; con risoluzione invece si intende la capacità di distinguere masse che differiscono di poco. Le tre componenti di questo strumento sono: la sorgente, dove avviene la ionizzazione delle molecole; l'analizzatore, dove avviene la separazione e l'analisi degli ioni in base al rapporto m/z; il rilevatore, dove arrivano gli ioni separati e si ha l'associazione con il valore m/z generando lo spettro di massa.
Nello studio in oggetto la LC/MS e la GC/MS sono usate ad esempio per l'analisi degli esperimenti eseguiti con isotipi come il $^{13}C_6$-glucosio.

2.3 RNA-sequencing (RNA-seq)

L'RNA-seq è una metodica che consente, tramite il sequenziamento randomico di frammenti di cDNA, di determinare sia i livelli di espressione genica (quindi l'abbondanza relativa) sia la struttura di trascritti di geni di interesse (esoni, introni e splicing alternativi). Si tratta quindi di una tecnica sia quantitativa che qualitativa. L'idea di base è quella di generare molte sequenze, molti frammenti, da allineare sul genoma di riferimento e tante più sequenze mapperanno su un gene, tanto più quel gene è espresso. Questa tecnica prevede vari passaggi, tra cui: il controllo della qualità del campione di RNA totale di partenza, l'eliminazione dell'rRNA, il sequenziamento e l'analisi dei dati.

2.3.1 Next Generation Sequencing – Illumina

In questo studio il sequenziamento randomico viene fatto utilizzando il *Next Generation Sequencing Illumina* che ha permesso di valutare i livelli espressione genica di varie proteine, come ad esempio di PHGDH.

L'Illumina è un sequenziatore di seconda generazione (progettato a seguito del sequenziatore di prima generazione Sanger) che si basa sulla tecnica del *sequencing by synthesis*. Rispetto al sequenziamento di prima generazione, viene saltato il clonaggio dei frammenti in plasmidi batterici, ma serve sempre amplificarli altrimenti la fluorescenza che emettono non sarebbe abbastanza intensa da essere rilevata (tappa non necessarianel sequenziamento di terza generazione).

I passaggi principali del metodo Illumina sono tre: preparazione dei frammenti, bridge PCR e *sequencing by synthesis*. In primis vengono generati i frammenti di cDNA che vengono poi uniti a due adattatori con sequenza diversa, mediante "ligazione". Questi adattatori sono caratterizzati dalla presenza al loro interno di una breve sequenza detta *index* in modo tale da rendere possibile il sequenziamento di campioni diversi, nella stessa reazione, e poi poterli distinguere. I frammenti a questo punto vengono denaturati e ibridati su una *flow cell*, un supporto costituito a sua volta da piccole cellette, all'interno delle quali sono presenti gli oligonucleotidi complementari alla sequenza degli adattatori. Questi oligonucleotidi fungono da primer per la *bridge PCR*, ovvero una *polymerase chain reaction* (PCR) che è caratterizzata dalla formazione di clusters di cloni, ciascuno dei quali si origina da una molecola di cDNA che si è ibridata.

La particolarità di questa tecnica è che in seguito all'estensione dei frammenti (con l'aggiunta di dNTPs e della polimerasi), essendo i primer legati al supporto, l'elica neosintetizzata, anch'essa legata, deve piegarsi per ibridarsi creando così un ponte che diventerà poi a doppia elica. Successivamente si denatura, così le due eliche si separano e si ripetono gli stessi passaggi fino alla formazione dei clusters. Infine, si fa il sequenziamento in parallelo dei singoli cloni tramite la tecnica del *sequencing by synthesis* che comprende: la denaturazione degli ampliconi generati, un lavaggio e poi l'aggiunta dei terminatori reversibili. I terminatori reversibili sono i quattro nucleotidi marcati con fluorofori diversi con all'estremità 3' un gruppo bloccante. Si procede poi con la rilevazione della fluorescenza: in base al colore della fluorescenza si definiscono i nucleotidi incorporati e quindi i corrispondenti sull'elica da sequenziare. Per determinare poi le basi successive, si rimuove il fluoroforo e il gruppo bloccante e si ripete il processo.

2.4 Modelli impiegati nello studio

2.4.1 Modelli in vitro: colture cellulari

Le colture cellulari consistono nel far crescere e proliferare linee cellulari in un ambiente controllato artificialmente, utilizzando appositi nutrienti. La principale linea cellulare impiegata nello studio è la linea umana di carcinoma ovarico A2780wt e la corrispondente linea resistente al cisplatino A2780cis.

2.4.2 Modelli in vivo: topi PDX (Patient Derived Xenografts)

In questo studio vengono utilizzati in molti esperimenti i modelli PDX, utili per studiare un tumore in diverse condizioni. Si tratta di modelli creati a partire da cellule o tessuti tumorali di pazienti, che vengono poi impiantati in topi immunocompromessi. È una forma di xenotrapianto, ovvero un trapianto fatto tra soggetti di specie diverse (in questo caso uomo e topo).
L'attecchimento del tessuto tumorale viene agevolato dall'immunodeficienza del topo in quanto riduce il problema del rigetto, ma dipende anche dall'origine del tumore stesso. Dato che il modello PDX conserva le caratteristiche del tumore primario del paziente, inclusi i profili di espressione genica e le risposte ai farmaci, si ritiene un modello di cancro umano in vivo molto affidabile.
In questo studio, i topi PDX sono stati usati per esempio per validare sia che l'esposizione alla chemioterapia a base di platino comporta la riduzione della biosintesi di serina, con ridotti livelli di PHGDH, sia per confermare la dipendenza delle cellule dalla serina esogena.

2.4.3 Modelli ex vivo: organoidi

Gli strumenti di ricerca in vitro sono sempre stati per la maggior parte rappresentati dalle colture cellulari, si tratta però di una tecnica che presenta dei limiti dal momento che dà informazioni abbastanza limitate sui processi biologici in vivo.
Con l'arrivo però di nuove tecniche è stato possibile avere in vitro potenti modelli tridimensionali: gli organoidi. Questa tecnologia permette di ricreare organi a partire da cellule staminali embrionali o pluripotenti, in una coltura appunto 3D. Ritrova diverse applicazioni, tra cui la medicina rigenerativa, la scoperta di farmaci, la medicina di precisione e funge da modello per le malattie.
In questo studio sono stati utilizzati organoidi derivati dai modelli PDX per studiare la resistenza alla chemioterapia a base di platino.

3. RISULTATI

Questo studio ha come scopo l'analisi del metabolismo della serina a seguito della chemioterapia a base di platino come trattamento per il cancro ovarico.
L'interesse per la via metabolica della biosintesi della serina deriva dal fatto che serina e glicina (derivata dalla serina) sono amminoacidi fondamentali per la produzione dei nucleotidi, necessari per l'aumento della proliferazione e del metabolismo cellulare. In molti degli esperimenti è stato infatti preso in esame lo studio di questa via metabolica, e in particolare i livelli dell'enzima PHGDH e la dipendenza dalla serina esogena. Sulla base dei risultati ottenuti, altri esperimenti mirano a comprendere il ruolo del NAD+ e degli enzimi PARP.

3.1 Diminuzione dell'espressione di PHGDH e ridotta attività biosintetica della serina nelle pazienti con recidiva resistente alla chemioterapia a base di platino

Lo studio parte da osservazioni ricavate dal dataset *The Cancer Genome Alta Program* (TCGA). All'interno del dataset sono stati selezionati i tumori ovarici resistenti al platino e come indice di attività biosintetica della serina sono stati valutati i livelli di espressione genica (mRNA) di PHGDH. I livelli significativamente più bassi sono stati riscontrati nelle pazienti resistenti rispetto a quelle sensibili [Fig. 4a]. Nella stessa coorte di pazienti norvegesi (n=9) si è osservata poi una correlazione tra riduzione dei livelli di PHGDH e sopravvivenza globale [Fig.4d], correlazione che è stata conferma anche in una coorte diversa, olandese, più numerosa (n=25) [Fig. 4f]. I grafici ottenuti mettono in relazione la percentuale di cambiamento dei livelli di PHGDH alla recidiva con la sopravvivenza globale della coorte.

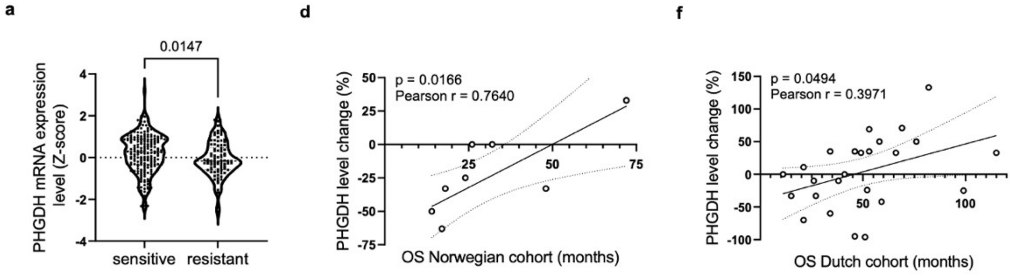

Figura 4: **a.** Espressione dei livelli di mRNA di PHGDH nelle pazienti con cancro ovarico nella coorte norvegese del TCGA; **d-f.** Correlazione tra variazioni dei livelli di PHGDH (%) e mesi di sopravvivenza globale (OS) nella coorte norvegese (d) e olandese (e). I valori del coefficiente di correlazione di Pearson per le due coorti sono rispettivamente r = 0.764 e r = 0.397. *Figura 1a, b, d dell'articolo in appendice.*

Per capire in quale misura l'espressione di questo enzima può cambiare durante lo sviluppo della resistenza, sono stati valutati i livelli proteici di PHGDH mediante immunoistochimica (IHC), utilizzando un approccio longitudinale. Sono state analizzate coppie di campioni prelevati dalla stessa paziente in due condizioni diverse: quando il tumore non era stato ancora trattato (*naive*) e in seguito all'acquisizione della resistenza al platino.

Queste analisi sono state condotte sulle due coorti sopra menzionate. In entrambi le coorti, alla recidiva corrisponde una down-regolazione del PHGDH, che correla con una ridotta sopravvivenza.
Per studiare l'attività biosintetica della serina è stata anche utilizzata la linea cellulare umana di carcinoma ovarico A2780wt e la corrispondente linea resistente al cisplatino A2780cis. Tramite Western blot e RNA-seq sono stati analizzati i livelli di espressione di PHGDH e di altri due enzimi coinvolti nella biosintesi della serina, PST1 e PSPH. I campioni sono stati valutati in diverse condizioni e i risultati hanno effettivamente mostrato che nella condizione di resistenza gli enzimi PHGDH e PST1 erano sottoregolati sia a livello di mRNA che di proteina e che PSPH era down-regolato solo a livello di proteina. Dal Western blot è possibile vedere che le bande sono molto ridotte nella linea *cis* (resistente) rispetto alla linea *wt* (sensibile) [Fig.5a]. Inoltre, tramite RNA-seq sono stati valutati anche i livelli dei trasportatori della serina (SLC1A4 e SLC1A5) che hanno messo in luce una loro sovra-espressione [Fig. 5b].

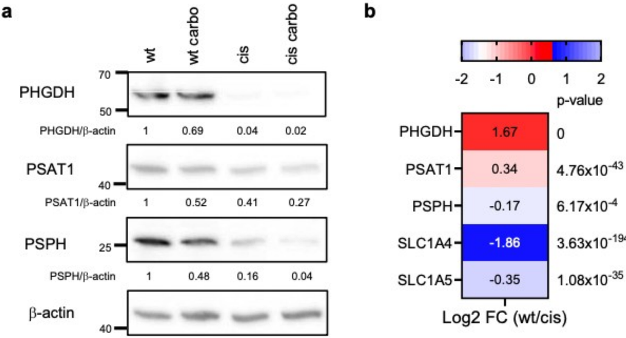

Figura 5: **a.** Western blot degli enzimi coinvolti nella via metabolica di biosintetica della serina nelle linee wt e cis, in assenza o in presenza di carboplatino (carbo); **b.** RNA-seq degli enzimi coinvolti nella via metabolica di biosintesi della serina e dei principali trasportatori della serina nel wt rispetto al cis (log2 fold change wt/cis). *Figura 2a, c dell'articolo in appendice.*

La down-regolazione della biosintesi della serina è stata inoltre studiata confrontando i livelli di PHGDH nei modelli murini di xenotrapianti derivati da pazienti (PDX) OVC1a (naive) e OVC1b (con recidiva dopo trattamento con platino) [Fig. 6b]. Inoltre, sono stati valutati i livelli anche nel modello OVC3 (da recidiva resistente) in assenza di trattamento (*vehicle*) o dopo ciclo chemio-recidiva-chemio (*relapse*).
Si è rilevato che nella condizione di recidiva i livelli di PHGDH sono nettamente più bassi [Fig. 6c].

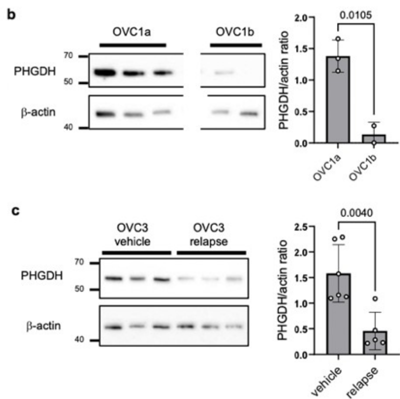

Figura 6: **b-c.** Western blot di PHGDH nei topi OVC1a e OVC1b (b) e OVC3 (c) con rispettive densitometrie. *Figura 4b, c dell'articolo in appendice.*

3.2 Le cellule resistenti sono auxotrofiche per la serina

Nelle linee A2780wt e A2780cis in presenza di isotopomeri del glucosio e di altri metaboliti sono stati poi studiati i cambiamenti metabolici associati alla resistenza e alla bassa espressione di PHGDH. Utilizzando tecniche di cromatografia gassosa (GC) e liquida (LC) accoppiate alla spettrometria di massa (MS), si è osservato che il processo di sintesi de novo della serina non è attivo nelle cellule resistenti e i livelli intracellulari di serina sono molto bassi. Inoltre, è stato anche evidenziato un aumento dell'assorbimento di glucosio e di serina dal mezzo di coltura, come atteso, considerata la maggiore espressione dei trasportatori di serina (SLC1A4 e SLC1A5). Gli autori dello studio hanno poi condotto degli esperimenti per indagare se la privazione di serina/glicina compromette la crescita cellulare. Utilizzando sempre la linea cellulare A2780wt e A2780cis si è visto che, in questa condizione, le cellule resistenti non crescono e che il fenotipo proliferativo viene recuperato solamente da un'integrazione di serina. Questo risultato evidenza quindi la richiesta di serina extracellulare per la sopravvivenza. Si è osservato anche che le cellule resistenti sottoposte ad una privazione prolungata di serina/glicina, vanno incontro ad adattamento e tornano a proliferare (in assenza di carboplatino). Le cellule con questo fenotipo, chiamate "cis serine synthesis pathway cells" (*cis SSP*), riattivano la biosintesi della serina, e rispetto alle cellule resistenti, mostrano in Western blot livelli più alti degli enzimi coinvolti in questa via metabolica. Si tratta quindi di un fenotipo in parte ri-sensibilizzato al carboplatino. Infine, anche la sovra-espressione di PHGDH nelle cellule resistenti in assenza di stress metabolico, induce una parziale ri-sensibilizzazione. Per confermare che in questo processo l'attività catalitica di PHGDH è essenziale, si è dimostrato che la sovra-espressione della forma inattiva dell'enzima, o "catalitically dead" (CD-PHGDH), non permette il fenotipo ri-sensibilizzato.

Queste conclusioni sono supportate anche da esperimenti in modelli PDX. In particolare, si è voluto verificare se la dieta priva di serina/glicina influenza in vivo la crescita di tumori con bassa attività biosintetica di serina. Il confronto è stato fatto tra il modello OVC1a (sensibile) e OVC2 (resistente). In quest'ultimo modello rispetto a OVC1a sono stati rilevati livelli inferiori sia di serina intracellulare che di PHGDH [Fig. 7], ed è stata osservata una crescita più lenta confermando l'ipotesi della dipendenza da serina esogena.

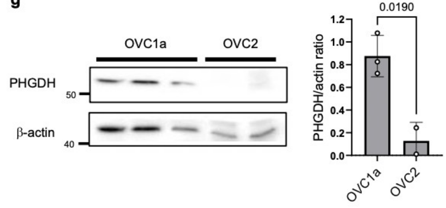

Figura 7: Western blot del PHGDH nei topi OVC1a e OVC2, con la rispettiva densitometria. *Figura 4g dell'articolo in appendice.*

3.3 Le cellule resistenti al platino riconfigurano le vie di rigenerazione del NAD+

Essendo la disponibilità di NAD+ uno dei principali vincoli per l'attività di PHGDH, è stato ipotizzato che le cellule resistenti possano spostare il metabolismo centrale del carbonio verso un fenotipo rigenerante NAD+ riducendo le attività che utilizzano NAD+, come la biosintesi della serina. Sono quindi stati misurati i livelli del rapporto NAD+/NADH e dei singoli cofattori in cellule sensibili e resistenti. Questi esperimenti hanno evidenziato che il rapporto NAD+/NADH e i livelli di NAD+ sono inferiori nelle cellule resistenti, confermando l'ipotesi del fenotipo che risparmia NAD+ [Fig. 8].

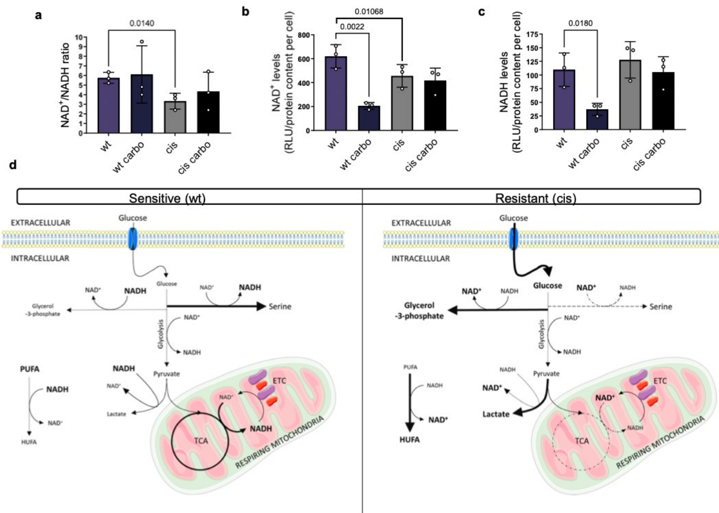

Figura 8: **a.** Rapporto NAD+/NADH. **b.** Livelli di NAD+. **c.** Livelli di NADH; **d.** Mappa metabolica che mostra le alterazioni metaboliche nelle cellule resistenti (cis) rispetto a quelle sensibili (wt), evidenziando che nelle cellule resistenti il NAD+ non viene utilizzato per la biosintesi della serina. *Figura 5a, b, c, d dell'artciolo in appendice.*

A questo punto è stato utilizzato l'inibitore della nicotinamide fosforibosiltransferasi (NAMPT, enzima quantitativamente più importante della sintesi NAD+), FK866, per studiare cosa accade alle cellule resistenti se sottoposte a trattamenti che vanno ad esaurire il NAD+. Confrontando l'effetto dell'inibitore in cellule sensibili e resistenti, il risultato è stato che entrambe sono sensibili, ma quelle resistenti lo sono circa il doppio. Infatti, la concentrazione per cui la proliferazione cellulare è inibita al 50% (GI50) è di 1.41 nM nelle cellule sensibili e 0.65 nM nelle cellule resistenti. Inoltre, si è visto che, una bassa dose di FK866, di per sé poco efficace compromette la proliferazione delle cellule resistenti se associata con il carboplatino [Fig. 9].

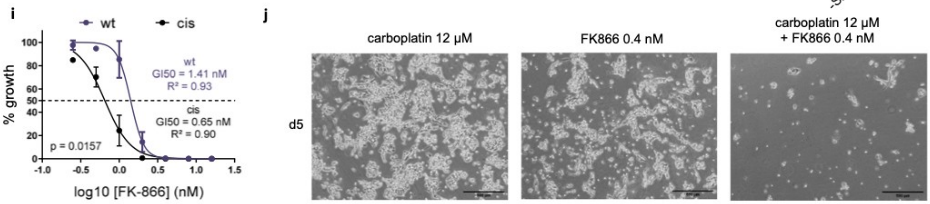

Figura 9: **i.** GI50 delle cellule wt e cis. **j.** Immagini rappresentative delle cellule cis rispettivamente sotto trattamento con solo carboplatino, solo l'inibitore FK866 e con la loro combinazione. *Figura 5i dell'articolo in appendice.*

3.4 Le cellule resistenti al platino aumentano l’attività dei PARP e l’inibizione di questi enzimi ri-sensibilizza le cellule al carboplatino

Come evidenziato dai risultati precedenti, nelle cellule resistenti si osserva un fenotipo che risparmia il NAD+, ma allo stesso tempo è stato anche osservato che non c’è un suo aumento a livello globale. Tenendo presente che gli enzimi PARP sono i principali consumatori di NAD+ nella riparazione del DNA, e che le cellule resistenti hanno una maggiore capacità di riparare il danno al DNA indotto da platino, è stato ipotizzato che queste cellule siano in grado di consumare più NAD+ attraverso l’attività dei PARP, spiegando così la discrepanza osservata.
La misura dei livelli di PARP1 (principale enzima PARP) evidenzia nelle cellule resistenti valori più elevati rispetto a quelle sensibili, sia in termini di proteina che di attività enzimatica [Fig. 10].

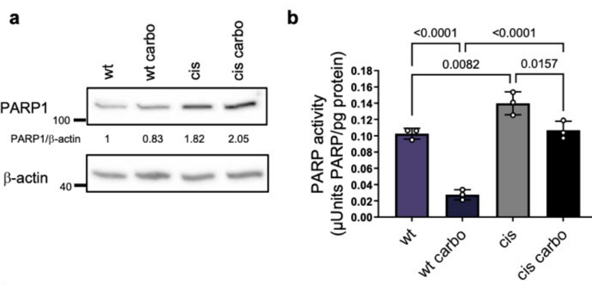

Figura 40: **a.** Western blot per la misurazione dei livelli di PARP1 in cellule wt e cis, trattate e non con carboplatino. **b.** Misurazione dell’attività enzimatica dei PARP. *Figura 6a, b dell’articolo in appendice.*

Inoltre, nelle cellule cis SSP (riattivate alla sintesi della serina) si è vista una riduzione dell’espressione di PARP1 e un aumento dei livelli di PHGDH. Ciò suggerisce che nelle cellule resistenti PHGDH e PARP competono per la disponibilità di NAD+.
Gli esperimenti successivi hanno indagato qual è l’effetto dell’inibizione farmacologica dei PARP nelle cellule resistenti esposte a trattamento con platino.
In particolare, l’effetto additivo degli inibitori dei PARP (in questo caso è stato utilizzato l’olaparib) in combinazione con carboplatino ha portato ad una diminuzione della proliferazione cellulare. In seguito, nello studio viene testata la combinazione inibitori PARP-carboplatino in vitro, sulla linea cellulare OVCAR3 (resistente). Anche in questo caso il risultato è stata la compromissione della crescita cellulare confermando che l’attività PARP svolge un ruolo importante nella sopravvivenza delle cellule resistenti, specificatamente sotto trattamento con carboplatino. È stata testata anche la combinazione olaparib con FK866 su cellule A2780cis e OVCAR3, ma, anche se la crescita cellulare rallentava, l’effetto era minore rispetto alla combinazione olaprib-carboplatino [Fig.11].

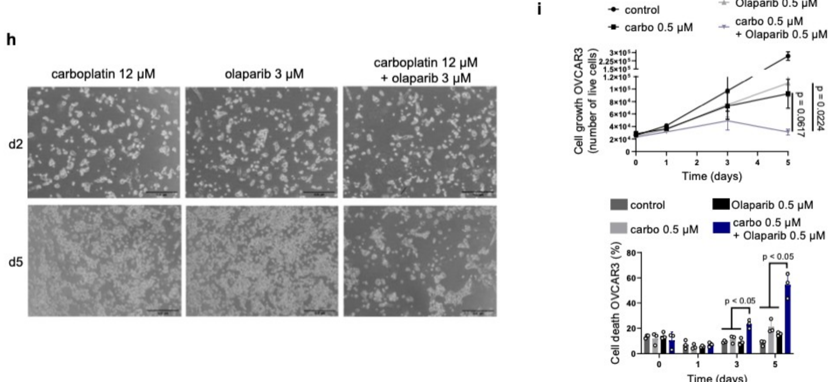

Figura 11: **h-i**. Immagini rappresentative delle cellule OVCA3 rispettivamente sotto trattamento con solo carboplatino, solo l'olaparib e con la loro combinazione. *Figura 6h, i dell'articolo in appendice.*

Infine, la combinazione di inibitori dei PARP e carboplatino, essendo risultata la più efficace, è stata testata in cellule organoidi derivate dai modelli PDX OVC4 e OVC5 resistenti, confermando l'effetto significativo di inibizione della crescita del tumore. Questi dati convalidano in campioni ex vivo i risultati in vitro, suggerendo che si può in parte ri-sensibilizzare il tumore al trattamento con platino inibendo l'attività dei PARP.
Dato che l'uso degli inibitori PARP è attualmente indicato per le recidive sensibili al platino, e per il mantenimento a seguito di terapia a base di platino per pazienti sensibili al platino con deficit di ricombinazione omologa (HRD), sono stati allora verificati gli stati mutazionali di diversi geni correlati alla ricombinazione omologa (HR) nei differenti modelli. I geni associati alla ricombinazione omologa sono vari, in particolare tra questi si ritrovano i geni BCAR1 e BCAR2. Per fare queste analisi è stato eseguito un sequenziamento dell'intero esoma (Whole Exome Sequencing, WES) nelle linee cellulari A2780 wt/cis e OVCAR3. I risultati ottenuti evidenziano che tutte le linee cellulari mostrano un carico mutazionale totale molto basso e solo mutazioni limitate nei geni correlati alla HR. Le stesse analisi fatte sui modelli PDX e sui loro organoidi derivati hanno mostrato invece una variabilità più alta nel carico totale mutazionale e nelle mutazioni correlate alla HR [Fig. 12]. Ciò suggerisce che le scoperte fatte sul potenziale della combinazione di carboplatino con gli inibitori dei PARP è indipendente dallo stato di HR dei differenti modelli.

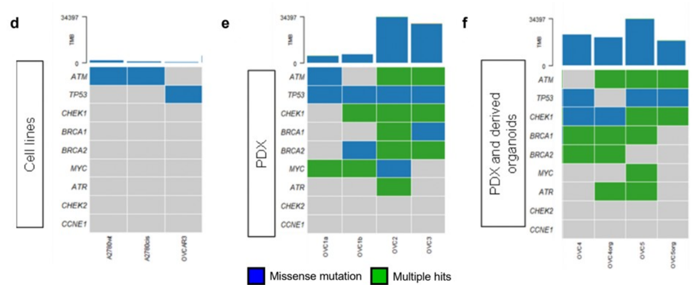

Figura 15: Analisi mutazionali dei principali geni correlati alla ricombinazione omologa nelle linee cellulari (**d**), nei modelli PDX (**e**) e negli organoidi associati ai modelli PDX (**f**). *Figura supplementare 8d, e, f dell'articolo in appendice.*

4. DISCUSSIONE

Lo sviluppo della resistenza alla chemioterapia a base di platino è un ostacolo importante nel trattamento del cancro ovarico e una delle principali cause di prognosi sfavorevole. L'articolo in esame dimostra che la riduzione della biosintesi della serina è uno dei principali adattamenti delle cellule resistenti. Queste ultime vanno così a preservare i livelli intracellulari di NAD+, in quanto la disponibilità di NAD+ limita l'attività del PHGDH. Allo stesso tempo è stato evidenziato come nelle cellule resistenti sia presente anche un livello elevato di PARP, gli enzimi che si occupano di riparare i danni al DNA. Dato che i PARP utilizzano in maniera consistente NAD+, esiste la possibilità che PARP e PHGDH competano per il coenzima NAD+ sotto stress indotto da platino. Un'osservazione simile è stata fatta in presenza di stress metabolico che induce la traslocazione di PHGDH nel nucleo, dove compete con PARP per il NAD+, modificandone l'attività trascrizionale (Ma et al., 2021).

Per quanto riguarda i dati derivati da campioni clinici, raccolti alla diagnosi e alla ricaduta, e i dati derivati dai modelli PDX, questi confermano che il fenotipo caratterizzato da bassi livelli di PHGDH può essere acquisito in un sottogruppo di pazienti che hanno sviluppato la resistenza, a seguito di successivi cicli terapeutici a base di platino (indipendentemente dai livelli originari di PHGDH). Queste osservazioni risultano importanti dal momento in cui molte pazienti, durante il decorso della malattia, vanno incontro a diversi cicli di risposta-ricaduta.
I risultati ottenuti dallo studio mostrano come la riduzione della via biosintetica della serina porta le cellule resistenti ad essere auxotrofiche per questo amminoacido. Infatti, in condizione di privazione di serina viene compromessa la crescita di queste cellule, sottolineando l'importanza della presenza di serina extracellulare. A partire da queste osservazioni si potrebbero progettare delle terapie che abbiano come scopo quello di rallentare la crescita tumorale andando ad agire sulla dieta. Inoltre, da questi risultati si può concludere che l'attività biosintetica della serina e in particolare i livelli di PHGDH e di serina intratumorale potrebbero essere utilizzati per fare previsioni sullo sviluppo della resistenza al platino. Per convalidare questi risultati sarà necessario avviare ulteriori studi di confronto di biopsie raccolte in maniera prospettica e longitudinale da una serie più ampia di pazienti.

I risultati ottenuti indicano che gli inibitori di PARP o della sintesi di NAD+, in combinazione con la chemioterapia a base di platino, potrebbero essere utilizzati nelle pazienti che presentano resistenza caratterizzata da una riduzione della biosintesi di serina. Se si considera poi che gli inibitori di PARP sono attualmente in uso nella terapia di mantenimento e che, in futuro, verranno utilizzati anche nelle fasi iniziali della terapia, l'adozione degli inibitori della sintesi del NAD+ potrebbe consentire di superare lo sviluppo di resistenze acquisite agli inibitori di PARP.

Un notevole passo avanti nella terapia personalizzata è stato infatti l'impiego degli inibitori di PARP come terapia di mantenimento per le pazienti con recidive sensibili al platino e con mutazioni nei geni BRCA, ossia in quei geni che codificano per proteine coinvolte nel meccanismo di riparazione HRR ("Homologous Recombination Repair").

Inoltre, l'evidenza clinica mostra che anche le pazienti senza mutazioni nei geni BRCA o senza deficit di ricombinazione omologa (HRD) potrebbero trarre beneficio dagli inibitori di PARP (González-Martín et al., 2019). Quest'aspetto è stato approfondito in questo studio esaminando lo stato mutazionale complessivo dei geni correlati alla HR (di cui le mutazioni nei geni BRCA1 e BRCA2 rappresentano una parte) tramite sequenziamento dell'intero esoma (WES). Dal momento che i dati ottenuti mostrano una grande variabilità nel carico mutazionale totale e nelle mutazioni correlate alla HR, sia nei modelli PDX che negli organoidi derivati da questi ultimi, si può concludere che la risposta alla combinazione carboplatino-olaparib nelle pazienti resistenti è indipendente dall'HRD. Questa non dipendenza dall'HRD rappresenta un enorme vantaggio, in quanto permetterebbe l'applicazione di questo approccio ad una platea più grande di pazienti e di tipologia di tumori, e non essere limitato solo alle pazienti HRD positive.

In conclusione, si può affermare che la biosintesi della serina ha un ruolo centrale nell'oncologia, ed è infatti noto da tempo che un suo aumento correla con la crescita del tumore, e che, al contrario, è stato da poco dimostrato che una sua riduzione favorisce lo sviluppo di metastasi (Rossi et al., 2022). A livello biochimico ciò si traduce con livelli di attività più alti e più bassi dell'enzima PHGDH. Il ruolo della biosintesi della serina nello sviluppo della resistenza alla chemioterapia è invece ancora poco indagato.
Il lavoro in esame apre una prospettiva importante in questa direzione, sia relativamente ai meccanismi di base sia per quanto riguarda la sperimentazione clinica e nuovi bersagli terapeutici. In particolare, questo studio rivela una vulnerabilità dal punto di vista metabolico che riguarda quel sottogruppo di pazienti con tumore ovarico, resistenti alla chemioterapia a base di platino, in cui l'entità della sotto-regolazione dei livelli di espressione di PHGDH (e quindi una riduzione della biosintesi della serina) correla con una prognosi peggiore. Ulteriori studi, oltre che approfondire questo argomento, in relazione anche alla dipendenza di serina extracellulare, potranno ad indagare se questo tipo di correlazione è presente anche in altri tipi di tumore. Molto interessante potrebbe essere l'impiego della tecnica di iso-imaging, che permetterebbe di valutare l'eterogeneità spaziale del metabolismo della serina, e quindi l'eterogeneità dei livelli di PHGDH.

BIBLIOGRAFIA

- Amelio, I., Cutruzzolá, F., Antonov, A., Agostini, M., & Melino, G. (2014). Serine and glycine metabolism in cancer. *Trends in Biochemical Sciences*, *39*(4), 191–198. https://doi.org/10.1016/j.tibs.2014.02.004

- Diehl, F. F., Lewis, C. A., Fiske, B. P., & Vander Heiden, M. G. (2019). Cellular redox state constrains serine synthesis and nucleotide production to impact cell proliferation. *Nature Metabolism*, *1*(9), 861–867. https://doi.org/10.1038/s42255-019-0108-x

- González-Martín, A., Pothuri, B., Vergote, I., DePont Christensen, R., Graybill, W., Mirza, M. R., McCormick, C., Lorusso, D., Hoskins, P., Freyer, G., Baumann, K., Jardon, K., Redondo, A., Moore, R. G., Vulsteke, C., O'Cearbhaill, R. E., Lund, B., Backes, F., Barretina-Ginesta, P., … PRIMA/ENGOT-OV26/GOG-3012 Investigators. (2019). Niraparib in Patients with Newly Diagnosed Advanced Ovarian Cancer. *The New England Journal of Medicine*, *381*(25), 2391–2402. https://doi.org/10.1056/NEJMoa1910962

- Lheureux, S., Braunstein, M., & Oza, A. M. (2019). Epithelial ovarian cancer: Evolution of management in the era of precision medicine. *CA: A Cancer Journal for Clinicians*, *69*(4), 280–304. https://doi.org/10.3322/caac.21559

- Liberti, M. V., & Locasale, J. W. (2016). The Warburg Effect: How Does it Benefit Cancer Cells? *Trends in Biochemical Sciences*, *41*(3), 211–218. https://doi.org/10.1016/j.tibs.2015.12.001

- Ma, C., Zheng, K., Jiang, K., Zhao, Q., Sha, N., Wang, W., Yan, M., Chen, T., Zhao, Y., & Jiang, Y. (2021). The alternative activity of nuclear PHGDH contributes to tumour growth under nutrient stress. *Nature Metabolism*, *3*(10), 1357–1371. https://doi.org/10.1038/s42255-021-00456-x

- Newman, A. C., & Maddocks, O. D. K. (2017). One-carbon metabolism in cancer. *British Journal of Cancer*, *116*(12), 1499–1504. https://doi.org/10.1038/bjc.2017.118

- Rossi, M., Altea-Manzano, P., Demicco, M., Doglioni, G., Bornes, L., Fukano, M., Vandekeere, A., Cuadros, A. M., Fernández-García, J., Riera-Domingo, C., Jauset, C., Planque, M., Alkan, H. F., Nittner, D., Zuo, D., Broadfield, L. A., Parik, S., Pane, A. A., Rizzollo, F., … Fendt, S.-M. (2022). PHGDH heterogeneity potentiates cancer cell dissemination and metastasis. *Nature*, *605*(7911), 747–753. https://doi.org/10.1038/s41586-022-04758-2

- Stewart, C., Ralyea, C., & Lockwood, S. (2019). Ovarian Cancer: An Integrated Review. *Seminars in Oncology Nursing*, *35*(2), 151–156. https://doi.org/10.1016/j.soncn.2019.02.001

- Yang, M., & Vousden, K. H. (2016). Serine and one-carbon metabolism in cancer. *Nature Reviews. Cancer*, *16*(10), 650–662. https://doi.org/10.1038/nrc.2016.81

APPENDICE

Van Nyen T, Planque M, van Wagensveld L, Duarte JAG, Zaal EA, Talebi A, Rossi M, Körner PR, Rizzotto L, Moens S, De Wispelaere W, Baiden-Amissah REM, Sonke GS, Horlings HM, Eelen G, Berardi E, Swinnen JV, Berkers CR, Carmeliet P, Lambrechts D, Davidson B, Agami R, Fendt SM, Annibali D, Amant F. Serine metabolism remodeling after platinum-based chemotherapy identifies vulnerabilities in a subgroup of resistant ovarian cancers. Nat Commun. 2022 Aug 5;13(1):4578. doi: 10.1038/s41467-022-32272-6. PMID: 35931688; PMCID: PMC9355973.

nature communications

Article

https://doi.org/10.1038/s41467-022-32272-6

Serine metabolism remodeling after platinum-based chemotherapy identifies vulnerabilities in a subgroup of resistant ovarian cancers

Received: 29 March 2022

Accepted: 19 July 2022

Published online: 05 August 2022

Tom Van Nyen[1,2], Mélanie Planque[3,4], Lilian van Wagensveld[5,6,7], Joao A. G. Duarte[3,4], Esther A. Zaal[8,9], Ali Talebi[10], Matteo Rossi[3,4], Pierre-René Körner[2], Lara Rizzotto[11], Stijn Moens[1], Wout De Wispelaere[1], Regina E. M. Baiden-Amissah[1], Gabe S. Sonke[12], Hugo M. Horlings[13], Guy Eelen[14], Emanuele Berardi[15], Johannes V. Swinnen[10], Celia R. Berkers[8,9], Peter Carmeliet[14,16,17], Diether Lambrechts[18,19], Ben Davidson[20,21], Reuven Agami[2,22], Sarah-Maria Fendt[3,4], Daniela Annibali[1,2,25] ✉ & Frédéric Amant[1,23,24,25] ✉

Resistance to platinum-based chemotherapy represents a major clinical challenge for many tumors, including epithelial ovarian cancer. Patients often experience several response-relapse events, until tumors become resistant and life expectancy drops to 12–15 months. Despite improved knowledge of the molecular determinants of platinum resistance, the lack of clinical applicability limits exploitation of many potential targets, leaving patients with limited options. Serine biosynthesis has been linked to cancer growth and poor prognosis in various cancer types, however its role in platinum-resistant ovarian cancer is not known. Here, we show that a subgroup of resistant tumors decreases phosphoglycerate dehydrogenase (PHGDH) expression at relapse after platinum-based chemotherapy. Mechanistically, we observe that this phenomenon is accompanied by a specific oxidized nicotinamide adenine dinucleotide (NAD^+) regenerating phenotype, which helps tumor cells in sustaining Poly (ADP-ribose) polymerase (PARP) activity under platinum treatment. Our findings reveal metabolic vulnerabilities with clinical implications for a subset of platinum resistant ovarian cancers.

Resistance to conventional chemotherapy is an obstacle for the treatment of many cancer types[1]. Epithelial ovarian cancer, the second most lethal gynecological malignancy worldwide[2], is a paradigmatic example. For more than four decades, standard of care first-line treatment is debulking surgery and platinum-based chemotherapy, and 5 years-overall survival rates remain close to 45%. High-grade serous carcinoma (HGSC) accounts for 70% of all ovarian cancer cases and most of the deaths. Although initial response to chemotherapy is very high (~80%), eventually patients relapse and succumb to platinum-resistant disease[3]. Over the years, important steps have led to a better understanding of the biology underlying resistance to platinum, but they have had only modest clinical impact and for resistant patients treatment objectives remain disease control and palliation[4–7].

A full list of affiliations appears at the end of the paper. ✉e-mail: daniela.annibali@kuleuven.be; frederic.amant@uzleuven.be

Metabolic alterations (e.g., Warburg effect, addiction to glutamine, or increased serine biosynthesis) have been linked to tumor development and maintenance in different cancer types[8–12]. Since metabolism is intertwined to signaling pathways controlling cell death[13], it is becoming more evident that metabolic adaptations may also support resistance to both chemotherapeutics and targeted agents[14–16]. Multiple and different traits, involving adaptations in both glucose and glutamine metabolism, and mitochondrial activity have been associated with platinum resistance in ovarian cancer cells[17–19]. Nevertheless, a concrete plan for their clinical translatability is still missing. Recent reports highlighted the role that reprogramming of the metabolism of certain amino acids might play in tumor adaptation to environmental cues and eventually in anticancer drug response[20]. The biosynthesis of serine from glucose, mediated by phosphoglycerate dehydrogenase (PHGDH), is one of the most studied metabolic pathways and it has been linked to development and progression of different cancer types[12,21–24]. Of note, it has been shown that primary and metastatic breast cancers differ in their serine biosynthetic requirements for molecular pathways activation, and that this may influence their sensitivity to specific targeted therapies[25], while heterogeneous and lower PHGDH expression potentiates tumor dissemination and metastasis formation in breast cancer[26]. However, the relevance of PHGDH expression and serine biosynthesis activity in tumors that acquire resistance after platinum exposure is largely unexplored.

Analyzing matched samples collected longitudinally during disease course, we found that a subgroup of ovarian cancer patients relapsed after platinum-based chemotherapy are characterized by decreased intratumor PHGDH levels, and that the extent of such decrease correlates with worse prognosis. We observed in in vitro preclinical models that PHGDH downregulation is accompanied by a general switch in the central carbon metabolism regulating NAD^+ availability, and that this may help to sustain PARP activity under platinum-based treatment. Consequently, combining carboplatin and PARP or NAD^+ synthesis inhibitors affects the growth of resistant models with decreased serine synthesis activity. Together, our results identify alterations in NAD^+ and serine metabolism as actionable vulnerabilities of a fraction of ovarian tumors adapting after platinum exposure, and provide a rationale to test new therapeutic approaches to overcome resistance.

Results

Decrease in PHGDH expression at relapse after platinum-based chemotherapy identifies a subset of ovarian cancer patients

To investigate serine biosynthetic activity in platinum-resistant ovarian cancers, we assessed gene expression levels of PHGDH (mRNA) in the original HGSC dataset from TCGA[27], with n = 287 newly diagnosed cases reporting platinum status. These data showed heterogeneity in PHGDH levels in chemo-naïve tumors, and that surprisingly patients who relapsed within 6 months since their last platinum treatment (clinically resistant cases, platinum-free interval PFI < 6 months, n = 90) had significantly lower PHGDH mRNA expression than the sensitive ones (PFI > 6 months, n = 197) (Fig. 1a). To investigate to what extent PHGDH expression might change during the process of developing resistance to platinum, we assessed PHGDH protein levels by immunohistochemistry (IHC) on pairs of archival effusion specimens sampled in the primary setting (chemo-naïve) and at the moment they were declared resistant, from nine distinct HGSC patients who received standard of care platinum-based chemotherapy as first-line treatment at the University of Oslo, Norway (Supplementary Table 1). Scoring from an expert pathologist showed that 6 out of 9 patients had decreased PHGDH levels at recurrence, while in 2 patients PHGDH scores did not change and only 1 had increased PHGDH at recurrence (Fig. 1b, c and Supplementary Fig. 1a, b and Supplementary Table 1). Although all patients died of disease, the four patients with the most pronounced decrease in PHGDH (pair 3, 5, 6 and 7) had the lowest overall survival (Fig. 1d and Supplementary Table 1). These data show that PHGDH downregulation may occur during disease progression in a subgroup of platinum-resistant ovarian tumors, and that the extent of decrease correlated with worse survival. We then sought to validate our findings in a second, larger cohort of patients from The Netherlands Cancer Institute (Amsterdam, The Netherlands). Since currently a large number of newly-diagnosed patients receive neoadjuvant platinum-based therapy, this new and more heterogeneous cohort consisted of 25 paired tumor tissue biopsies, collected at diagnosis (primary debulking or after neoadjuvant platinum treatment), and at relapse (early or late) (Fig. 1b and Supplementary Table 2). In this Dutch cohort, scored independently by a second expert pathologist, we also observed that PHGDH downregulation at recurrence was an appreciable phenomenon (Fig. 1b, e and Supplementary Fig. 1c, d and Supplementary Table 2), with PHGDH scores decreased in 11 patients, increased in 12 patients, and unchanged in 2 patients. In addition, patients with decreased PHGDH scores at recurrence had lower overall survival, compared to patients who had increased PHGDH scores (Supplementary Fig. 1e and Supplementary Table 2) and we confirmed the correlation between the extent of PHGDH levels decrease and overall survival (Fig. 1f). Together, we found that PHGDH downregulation is an event happening in ~44–67% of the patients who received platinum-based chemotherapy in two independent cohorts of longitudinally-collected paired biopsies. This suggests that decreased PHGDH expression at recurrence after platinum exposure, independent of primary PHGDH levels, could be associated to development of resistance.

Platinum-resistant ovarian cancer cells characterized by decreased serine biosynthetic activity are auxotrophic for serine

We then hypothesized that platinum exposure could remodel serine metabolism. To further investigate serine metabolism in acquired platinum resistance while mimicking the setting of our clinical paired datasets, we used the A2780wt cell line and its isogenic resistant counterpart A2780cis, originally established by chronically exposing parental cells to cisplatin[28], and tested their response to carboplatin. Resistant cells grew slower than parental cells but were able to sustain proliferation under acute carboplatin treatment, reflected in their GI50 values (17.09 ± 1.11 μM for cis and 2.85 ± 1.11 μM for wt cells, respectively) (Supplementary Fig. 2a). Next, we analyzed the expression of the three serine biosynthetic enzymes and found that PHGDH and phosphoserine aminotransferase (PSAT1) were downregulated in resistant cells compared to sensitive cells both at the protein (Fig. 2a) and mRNA level (Fig. 2b), while phosphoserine phosphatase (PSPH) expression was decreased only at the protein level (Fig. 2a, b), suggesting a post-transcriptional regulation for this specific enzyme. To investigate the metabolic changes associated with resistance and low PHGDH expression, we supplemented both cell lines with $^{13}C_6$-glucose and extracted metabolites at day 5 of carboplatin treatment (Supplementary Fig. 2b). Abundance of specific metabolites (i.e., glycolytic and TCA intermediates, amino acids and lipids) was altered in sensitive cells under treatment but also in untreated resistant cells, suggesting that sensitive cells undergo metabolic changes after platin exposure, and that specific rearrangements could be associated with acquired resistance (Supplementary Fig. 2c). Specifically, we detected striking alterations in the isotopomer distributions of serine and glycine derived from $^{13}C_6$-glucose (Fig. 2c–e), with resistant cells showing almost no incorporation of ^{13}C in any of the two amino acids compared to sensitive cells (Fig. 2d, e), indicating that the process of de novo serine (and glycine) synthesis from glycolytic intermediates was not active in A2780 cells once they acquired resistance (Supplementary Fig. 2d). In resistant cells, downregulation of serine biosynthesis correlated with lower intracellular abundance of both serine and glycine (Fig. 2f, g). In addition, we observed increased glucose uptake (Fig. 2h) in resistant cells, suggesting that the decreased glucose-derived

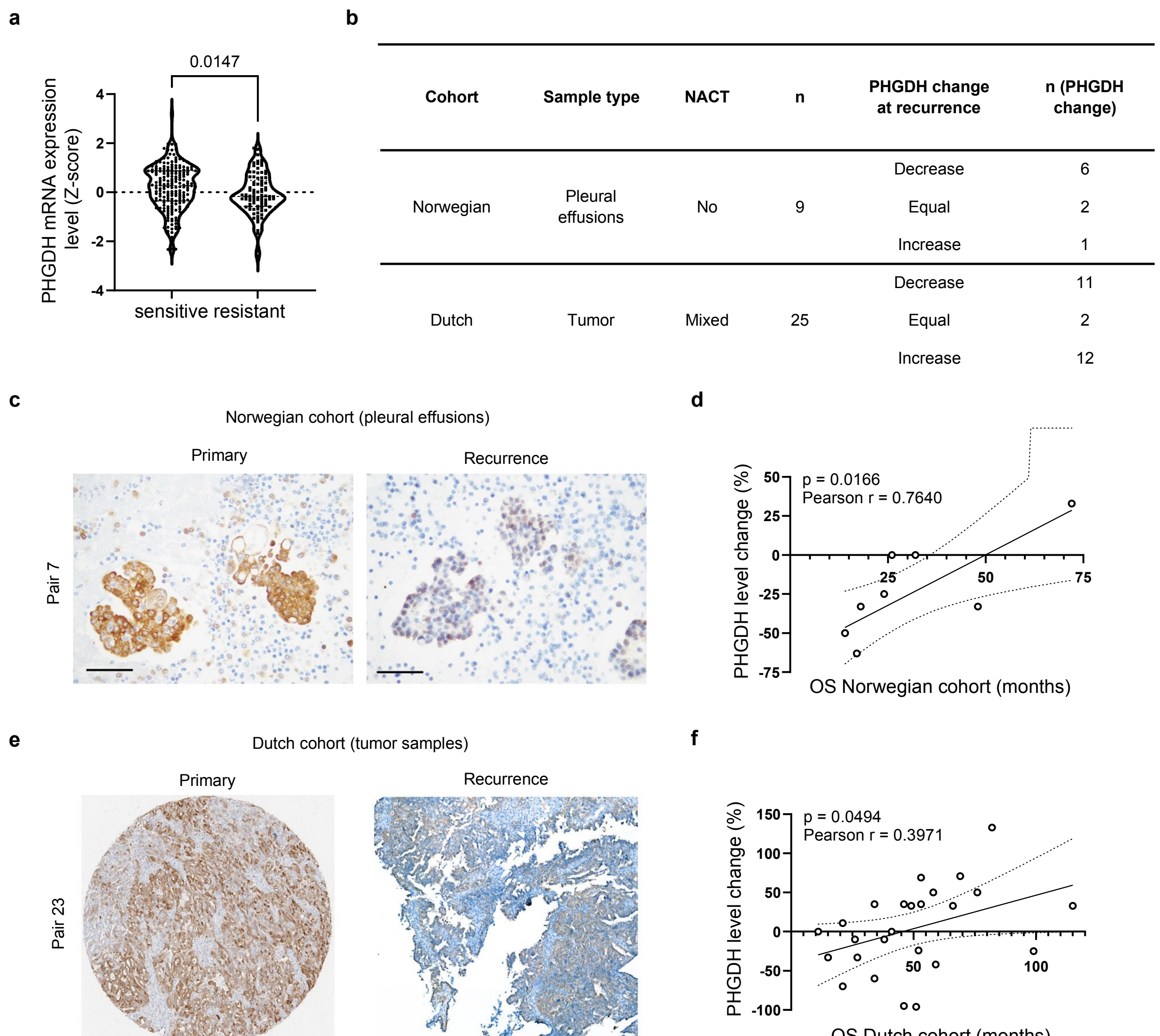

Cohort	Sample type	NACT	n	PHGDH change at recurrence	n (PHGDH change)
Norwegian	Pleural effusions	No	9	Decrease	6
				Equal	2
				Increase	1
Dutch	Tumor	Mixed	25	Decrease	11
				Equal	2
				Increase	12

Fig. 1 | Decrease in PHGDH expression after platinum-based chemotherapy identifies a subset of ovarian cancer recurrences. a PHGDH mRNA expression levels of ovarian cancer patients in the TCGA cohort, n = 197 sensitive patients and n = 90 resistant patients, unpaired two-tailed t-test. b Overview of the Norwegian and Dutch patient cohort and related PHGDH changes, NACT neoadjuvant chemotherapy. c Example of PHGDH IHC staining of primary and late recurrent clinical specimen of the Norwegian cohort, scale bar is 50 µm. d Correlation of PHGDH protein level change at recurrence and overall survival in the Norwegian cohort, simple linear regression determined by minimizing sum of squares is shown with 95% confidence bands, Pearson correlation r = 0.7640 and p = 0.0166. e Example of PHGDH IHC staining of primary and recurrent clinical specimen of the Dutch cohort, scale bar is 500 µm. f Correlation of PHGDH protein level change at recurrence and overall survival in the Dutch cohort, simple linear regression determined by minimizing sum of squares is shown with 95% confidence bands, Pearson correlation r = 0.3971 and p = 0.0494. Source data are provided as a Source Data file. NACT neoadjuvant chemotherapy, OS overall survival.

carbons flux through the serine synthesis pathway (SSP) was not the consequence of lower intracellular glucose availability, but a peculiar metabolic adaptation. We also observed that resistant cells took up twice more serine from the medium, compared to the sensitive ones (Fig. 2i), as expected due to the higher expression of two major serine transporters, SLC1A4 and SLC1A5 (Fig. 2b), while this was not the case for other amino acids or for glycine, which was on the contrary excreted in the medium (Supplementary Fig. 2e). Of note, metabolic analysis at an early time point, after 24 h, showed the same trends observed analyzing ^{13}C labeling at steady-state after 5 days (Supplementary Fig. 2f–h). Together, these data show that the acquisition of resistance to platinum in A2780 cells is associated with de novo serine synthesis downregulation and with an adaptive increase in extra-cellular serine uptake.

Resistant A2780 cells require exogenous serine for nucleotides production and proliferation

Since our data showed that A2780cis cells do not synthetize serine, we then asked whether serine/glycine starvation could impair their growth and viability and observed that resistant cells deprived of serine and glycine did not proliferate (Fig. 2j), while sensitive cells continued to grow (Supplementary Fig. 3a). Supplementation of 0.093 mM serine, a fraction equivalent to 1/3 of the amount originally present in conventional medium (0.28 mM), was enough to fully recover the proliferative phenotype, while glycine supplementation was not, in line with what has been reported by Labuschagne et al. for different cells deprived from serine (Fig. 2j) [29]. Carboplatin treatment synergized with serine starvation, leading to the death of resistant cells, a phenotype that was again completely rescued by re-

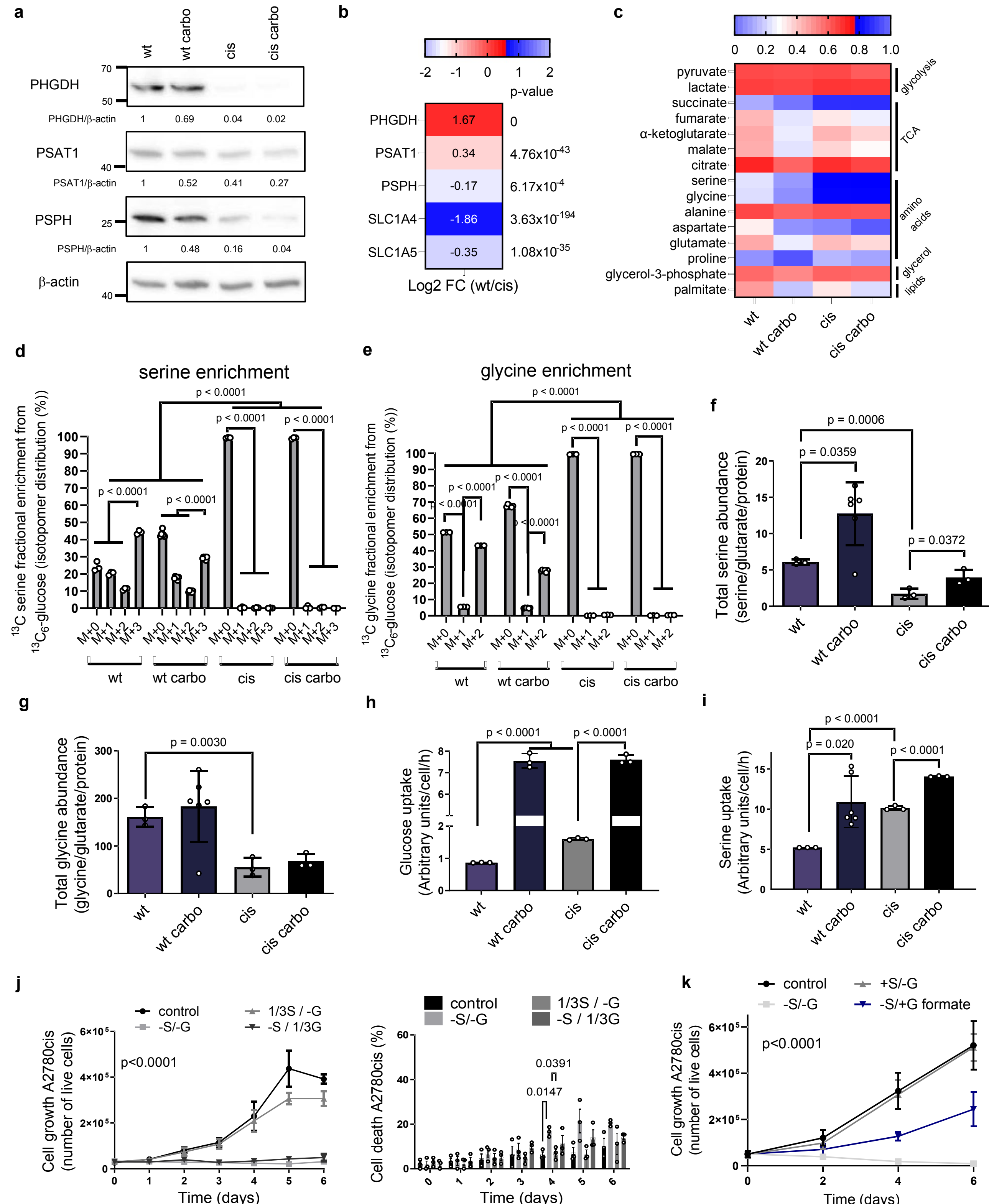

supplementing serine (Supplementary Fig. 3b). Thus, we concluded that resistant cells require extracellular serine to proliferate and survive platinum treatment.

Next, we asked whether serine/glycine deprivation selectively inhibited the growth of resistant cells by affecting their redox homeostasis, because we observed that platinum treatment induced oxidative stress in sensitive cells while resistant cells were able to better tolerate platinum-induced reactive oxygen species (ROS) (Supplementary Fig. 3c, d). In resistant cells we observed increased levels of both cytoplasmic and mitochondrial ROS, but only under serine/glycine starvation (Supplementary Fig. 3c, d). In line, carboplatin treatment synergized with serine/glycine deprivation to induce ROS accumulation in both sensitive and resistant cells at day 5 (Supplementary Fig. 3c, d). However, although N-acetyl-cysteine (NAC) supplementation was able to rescue survival and proliferation of the sensitive cells under carboplatin (Supplementary Fig. 3e), it had no

 https://doi.org/10.1038/s41467-022-32272-6

Fig. 2 | Ovarian cancer cells with acquired resistance after platinum exposure have low serine biosynthetic activity and are auxotrophic for serine. a Representative western blot of serine biosynthetic enzymes, n = 5 biological replicates. b Serine biosynthetic enzymes and main serine transporters enrichment in wt vs cis cells determined by RNA-seq analysis, mean values are represented, n = 3 technical replicates, p values obtained by DESeq2 (Wald-test with Benjamini and Hochberg multiple testing). c Glucose enriched metabolites in wt and cis cells with and without 6 μM carboplatin determined by GC-MS, median values are represented, representative figure of n = 3 technical replicates and n = 6 technical replicates for wt carbo (n = 2 biological replicates). Serine (d) and glycine (e) isotopomer distribution in cells grown with $^{13}C_6$-labeled glucose, representative figure of n = 3 technical replicates and n = 6 technical replicates for wt carbo (n = 2 biological replicates), ordinary two-way ANOVA with Tukey's multiple comparison post-test, data are represented as mean ± SD, p < 0.0001. Total serine (f) and glycine (g) levels determined by GC-MS with glutarate as internal standard and normalized to protein level, representative figure of n = 3 (n = 6 for wt carbo) technical replicates (n = 4 biological replicates), unpaired two-tailed t-tests, data are represented as mean ± SD. h Glucose uptake determined by LC-MS, n = 3 technical replicates, unpaired two-tailed t-tests, data are represented as mean ± SD. i Serine uptake determined by GC-MS, n = 3 (n = 6 for wt carbo) technical replicates, unpaired two-tailed t-tests, data are represented as mean ± SD. j Growth (left) and cell death (right) of cis cells under serine/glycine deprivation, determined with trypan blue exclusion assay, n = 3 biological replicates (with three technical replicates each), repeated measures two-way ANOVA, p < 0.0001 (left) and repeated measures two-way ANOVA with Tukey's multiple comparison post-test, p = 0.0393 (right), data are represented as mean ± SEM. k Growth of cis cells in serine/glycine deprived medium supplemented with 1 mM formate determined by trypan blue counting, n = 3 biological replicates (with three technical replicates each), repeated measures two-way ANOVA, data are represented as mean ± SD, p < 0.0001. Source data are provided as a Source Data file. FC fold change, Carbo carboplatin treated, S serine, G glycine, TCA tricarboxylic acid cycle.

effect on resistant cells starved from serine/glycine (Supplementary Fig. 3f). These results suggest that in resistant cells the oxidative stress measured under serine/glycine deprivation, unlike the one caused by carboplatin treatment in sensitive cells, is not the primary cause of the proliferative arrest but arises as consequence of an earlier metabolic imbalance.

Then, we investigated to what extent the proliferative arrest of resistant cells grown without serine/glycine was caused by their decreased ability to produce nucleotides. Since serine is a major donor of one-carbon (1C) units and can be converted to glycine, both necessary for synthetizing purine precursors and thymine (Supplementary Fig. 3g, h), we supplemented resistant cells with formate and glycine, to define whether proliferation can be restored in the absence of serine. We observed a partial rescue of proliferation when serine-starved resistant cells were supplemented with both formate and glycine (Fig. 2k), suggesting that resistant cells require exogenous serine to produce nucleotides, in agreement to what has been previously reported in different cancer cells [29]. To verify this, we grew sensitive and resistant cells in the presence of $^{13}C_3$-serine and observed labeling incorporation in ~70% of the purines and TMP in resistant cells, and only ~15–20% in the sensitive ones (Supplementary Fig. 3i–l). Together, these data show that A2780 resistant cells rely on exogenous serine to produce nucleotides and sustain proliferation.

Serine biosynthetic activity correlates with platinum responsiveness in A2780 resistant cells

Next, we investigated whether a longer starvation would result in a stronger effect, since 5 days of serine deprivation impaired proliferation specifically in resistant cells but did not induce cell death (Fig. 2J). After ±10 days in medium without serine/glycine, resistant cells adapted to bypass the growth arrest and started to proliferate again, when grown in the absence of carboplatin (Fig. 3a). These proliferating cells (named cis SSP cells) expressed serine biosynthetic enzymes, mainly PHGDH, at higher levels compared to the ones observed in resistant cells, both at protein and mRNA level (Fig. 3b, c). These data demonstrate that resistant cells could selectively switch their metabolism and re-activate serine biosynthesis from glucose in order to survive the amino acid deprivation, but only in the absence of platinum. As already reported for other cancer cell types under serine starvation [30,31], we observed that PHGDH re-expression was regulated at the transcriptional level following ATF4 upregulation at day 4, in serine/glycine-free medium (Fig. 3d). We then investigated whether serine biosynthesis re-activation would correlate with changes in platinum responsiveness. We found that cis SSP cells partially regained sensitivity to platinum when grown in serine/glycine depleted or complete medium, as shown by their GI50 value of 6.32 ± 1.04 μM and 8.42 ± 1.10 μM, respectively (Fig. 3e). These results show that resistant cells are able to re-activate serine synthesis, if subjected to the metabolic stress induced by serine deprivation, and this partly re-sensitize them to platinum. To assess whether PHGDH expression levels in resistant cells would correlate with carboplatin sensitivity also in full medium and not only under metabolic stress, we genetically overexpressed PHGDH (Fig. 3f), and verified that PHGDH overexpression partially re-sensitized resistant cells to carboplatin (Fig. 3g). This was not the case when we overexpressed the catalytically-inactive form of the enzyme (catalytic-dead PHGDH (CD-PHGDH)) (Fig. 3f, g), indicating that PHGDH catalytic function was essential for carboplatin re-sensitization.

We then investigated whether PHGDH downregulation in chemo-naïve sensitive cells would per se make them more resistant to carboplatin. To do this, we silenced it by means of two distinct shRNAs (shPHGDH1 and shPHGDH2, with downregulation to ~50% and ~10% of the original levels, respectively). Independently on the degree of silencing, PHGDH downregulation not only did not induce resistance in sensitive cells, but slightly increased their sensitivity to carboplatin (Supplementary Fig. 4a, b). Interestingly, we also observed that PHGDH downregulation was sufficient to induce DNA damage (Supplementary Fig. 4c, d) even in the absence of platinum, in agreement with what was observed in PHDGH^{high} subsets of lung cancer [24]. These data confirmed that PHGDH catalytic activity may influences platinum responsiveness in cells that acquired resistance after treatment, but not in sensitive, chemo-naïve cells.

Relapses after platinum-based chemotherapy exposure in patient-derived xenograft (PDX) models are characterized by decreased PHGDH expression

To validate our findings in vivo, we used clinically annotated PDXs established from ovarian cancer patients (Supplementary Fig. 5a and Supplementary Table 3). To test our hypothesis that exposure to platinum may induce a metabolic rewiring involving, among other processes, also downregulation of serine biosynthesis, we measured PHGDH levels in the OVC1a PDX model, established from a chemo-naïve platinum sensitive tumor, and in the matched OVC1b PDX model, established from the clinical relapse after platinum treatment in the same patient (Supplementary Table 3). In agreement with the observed clinical response, the OVC1b tumors in mice were still sensitive to platinum (Fig. 4a), but expressed lower levels of PHGDH (Fig. 4b), compared to OVC1a. Next, we tested the OVC3 PDX model, established from a patient that initially responded to platinum but relapsed within 6 months and was declared resistant (Supplementary Table 3). OVC3 initially respond to treatment, however the tumors in the mice relapsed between 6–15 weeks after the last platinum treatment, resembling the clinical response in the patient (Supplementary Fig. 5b). We analyzed PHGDH levels in vehicle-treated OVC3 mice and in OVC3 mice that underwent a chemo-relapse-chemo cycle, and we observed lower PHGDH levels in the relapsed samples, compared to the control ones (Fig. 4c and Supplementary Fig. 5b).

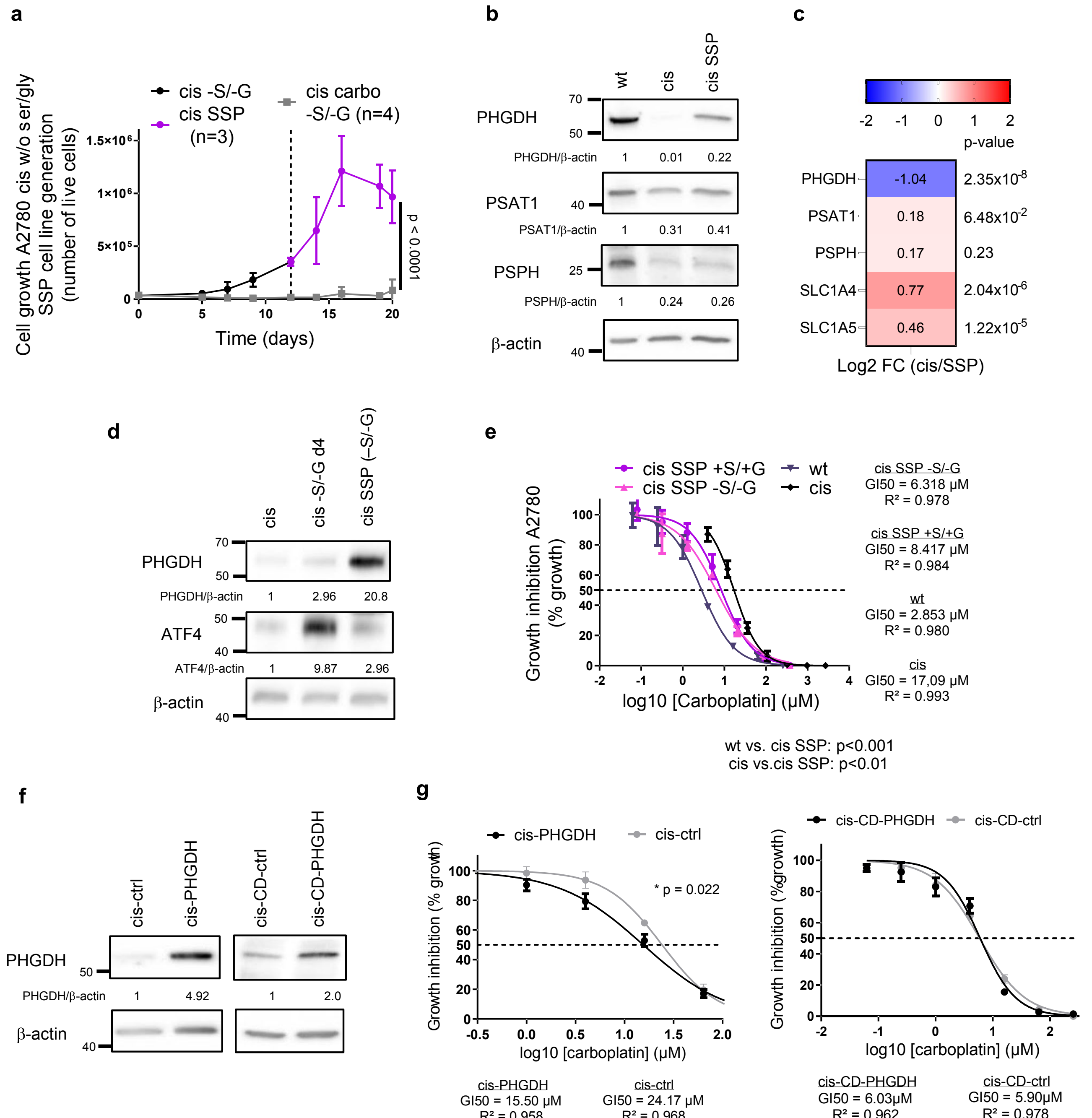

Fig. 3 | Serine biosynthetic activity correlates with platinum responsiveness in A2780 resistant cells. a Generation of cis SSP cell line established after serine/glycine deprivation of cis cells, n = 3 biological replicates for cis cells, n = 4 biological replicates for cis carbo cells (with three technical replicates each time), repeated measures two-way ANOVA, data are represented as mean ± SD. b Representative western blot of serine biosynthetic enzymes, n = 4 biological replicates. c RNA-seq results of serine biosynthetic enzymes and main transporters in cis SSP cells, mean values are plotted, n = 3 technical replicates, p values obtained by DESeq2 (Wald-test with Benjamini and Hochberg multiple testing). d Representative western blot of PHGDH and ATF4 in cis cells, serine and glycine starved cis cells and SSP cells, n = 2 biological replicates. e GI50 curves of wt, cis and cis SSP cells, n = 3 biological replicates (with three technical replicates each time), unpaired two-tailed t-tests between GI50 values, data are represented as mean ± SD, p = 0.0047 for cis vs. cis SSP +S/G and p = 0.0047 for wt vs. cis SSP −S/G. f Western blot of PHGDH and CD-PHGDH in genetic overexpressing cis cells, n = 3 biological replicates for cis-PHGDH and n = 2 biological replicates for cis-CD-PHGDH. g GI50 cuves of cis-control and cis-PHGDH overexpressing cells and cis-CD-control and cis-CD-PHGDH overexpressing cells, n = 4 biological replicates for cis-empty and cis-PHGDH and n = 3 biological replicates for cis-CD-empty and cis-CD-PHGDH (with three technical replicates each time), unpaired two-tailed t-tests between GI50 values, data are represented as mean ± SEM, p = 0.022 for cis-PHGDH vs cis-ctrl. Source data are provided as a Source Data file. Cis SSP serine synthesis pathway active cis cells, S serine, G glycine, CD catalytic dead.

Platinum-resistant PDX tumors with low serine biosynthetic activity depend on exogenous serine for optimal growth

To investigate whether serine and glycine deprivation can affect in vivo the growth of tumors with low serine biosynthetic activity, we compared two different PDX models, the sensitive OVC1a and the resistant OVC2 ($PHGDH^{low}$) model, and exposed them to serine/glycine-free diet. OVC2 was established from a patient with a resistant lesion that developed during years, after being exposed to different

https://doi.org/10.1038/s41467-022-32272-6

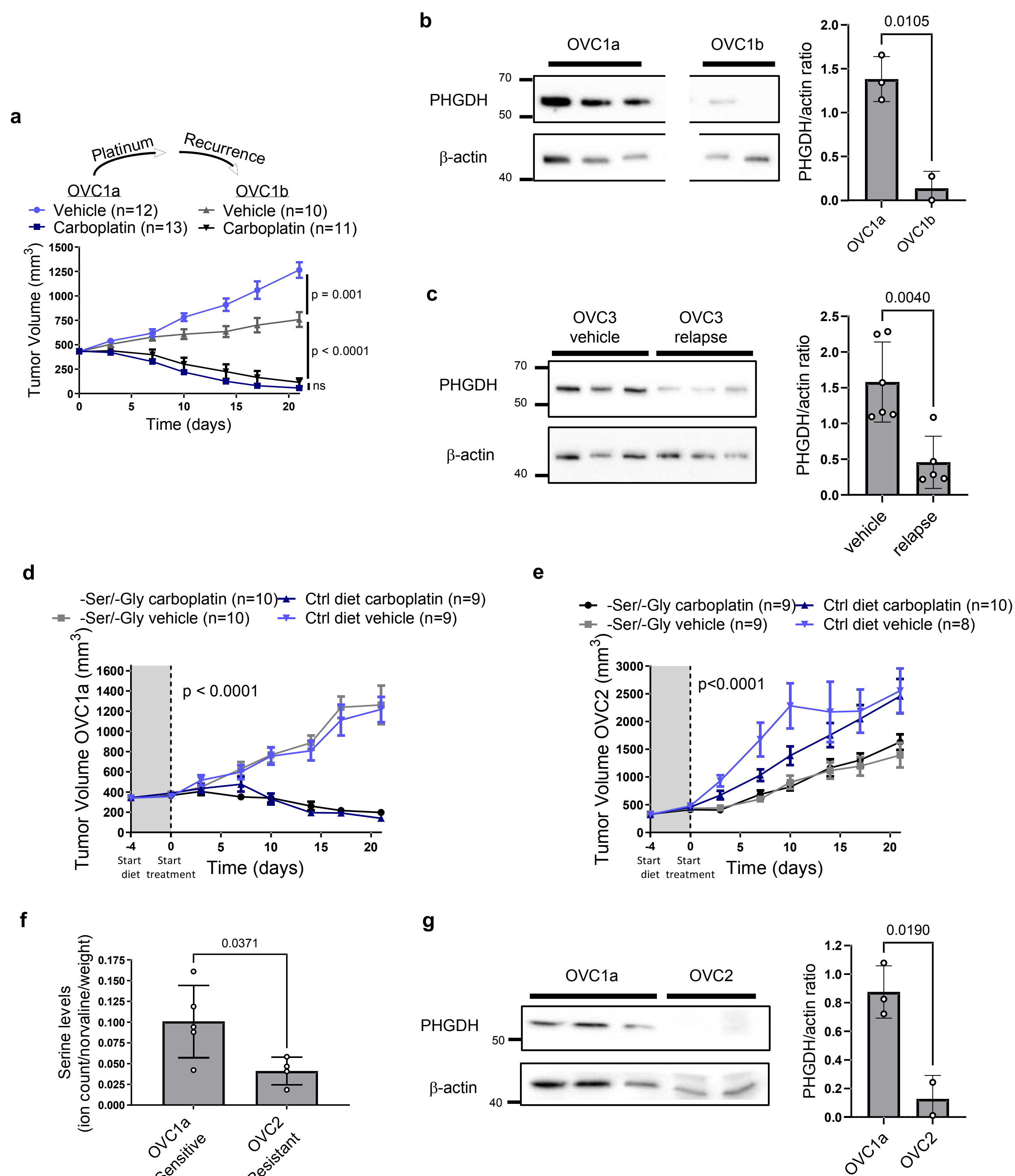

lines of platinum treatment (Supplementary Table 3). For both models we verified that response to platinum treatment effectively mimics the one observed in the original patient, with OVC1a tumors achieving complete response and OVC2 progressing under carboplatin treatment, respectively (Fig. 4d, e and Supplementary Table 3). We observed that resistant OVC2 tumors had significantly lower serine intracellular abundance and lower PHGDH levels, compared to the sensitive OVC1a ones (Fig. 4f, g). The serine/glycine-free diet increased the levels of all other amino acids in the plasma of our NMRI nude control mice, resulting in decreased relative serine and glycine levels, but did not decrease the absolute serine and glycine concentration (Supplementary Fig. 5c, d). This could be explained by the fact that circadian fluctuations in circulating serine levels are at a low in the afternoon, when all our samples have been collected (4–6 p.m.) and that immunocompromised mice seem to have higher basal plasma levels of serine, compared to the C57BL/6J mice[22]. Although we did not see a synergistic effect with carboplatin administration, suggesting that different—and maybe longer—diet protocols could be needed, we observed that also in vivo resistant tumors grew significantly slower upon serine/glycine-free diet, while the sensitive ones were not

Fig. 4 | Relapses after platinum exposure in PDX mice are characterized by decreased PHGDH expression and platinum-resistant PDX mice rely on exogenous serine for optimal growth. a Tumor response to carboplatin treatment of the sensitive OVC1a model and its sensitive relapse OVC1b, OVC1a vehicle-carboplatin, n = 12–13 mice, respectively; OVC1b vehicle-carboplatin n = 10–11 mice, respectively, repeated measures two-way ANOVA with multiple comparison Tukey's post-test, data are represented as mean ± SEM, $p < 0.0001$. b Representative western blot of PHGDH of OVC1a and OVC1b mice, n = 3 and n = 2 mice for OVC1a and OVC1b, respectively, and densitometric quantification, western blot was performed three times, unpaired two-tailed t-test, data are represented as mean ± SD, p = 0.0105. c Western blot of n = 3 vehicle-treated mice and n = 3 relapsed OVC3 mice after two rounds of carboplatin treatment and densitometric quantification of this western blot performed two times (n = 6 and n = 5 for vehicle and relapse, respectively), unpaired two-tailed t-test, data are represented as mean ± SD, p = 0.0040. d Tumor response to carboplatin treatment and serine/glycine-free diet in the sensitive OVC1a model, -ser/-gly diet: n = 10 vehicle and n = 10 carboplatin treated, control diet: n = 9 vehicle and n = 9 carboplatin treated, repeated measures two-way ANOVA, data are represented as mean ± SEM, $p < 0.0001$. e Tumor response to carboplatin treatment and serine/glycine-free diet in the resistant OVC2 model, -ser/-gly diet: n = 9 vehicle and n = 9 carboplatin treated, control diet: n = 8 vehicle and n = 10 carboplatin treated, repeated measures mixed-effects two-way ANOVA, data are represented as mean ± SEM, $p < 0.0001$. f Total serine levels in OVC1a (n = 5 mice) and OVC2 (n = 4 mice), unpaired two-tailed t-test, data are represented as mean ± SD, p = 0.0371. Total serine levels were determined three independent times. g Representative western blot of PHGDH of OVC1a (n = 3) and OVC2 (n = 2) mice and its densitometric quantification, unpaired two-tailed t-test, data are represented as mean ± SD, p = 0.0190. Western blot was performed three times. Source data are provided as a Source Data file.

affected by the diet (Fig. 4d, e). These data confirm that dependence on exogenous serine for fast proliferation is a metabolic feature of PHGDH-low expressing resistant tumors also in vivo.

Platinum-resistant cells rewire NAD^+-regenerating pathways

Although different tumor types have been reported to depend on serine biosynthesis for development and growth[12,23,25], our data suggest that under platinum pressure ovarian cancer cells may gain an advantage by selectively downregulating this process. We therefore sought to investigate how carbon flux through the serine biosynthetic pathway could functionally influence cellular response to platinum in our cells. Since the first reaction catalyzed by the rate limiting enzyme PHGDH consumes NAD^+ to produce 3-phosphohydroxypyruvate and it is well known that NAD^+ availability is a major constraint for PHGDH activity (Supplementary Fig. 2d)[32], we hypothesized that resistant cells may reduce carbons flux through serine synthesis at the level of PHGDH to spare NAD^+. We thus measured NAD^+/NADH ratio and the levels of the single cofactors in both sensitive and resistant cells and observed a lower NAD^+/NADH ratio and lower NAD^+ levels in resistant cells (Fig. 5a, b), with comparable NADH levels (Fig. 5c).

We then integrated our metabolomics data and found that resistant cells show a general metabolic rewiring toward a NAD^+-regenerating phenotype, in comparison to the naïve sensitive cells (Fig. 5d). While we did not find major differences in oxygen consumption rate (OCR) (Supplementary Fig. 6a), we observed that resistant cells were characterized by lower levels of TCA intermediates (Supplementary Fig. 2c) but sustained pyruvate carboxylase activity under treatment (Supplementary Fig. 6b), probably to replenish them (Supplementary Fig. 6c). We also measured higher lactate and adenosine-5′-triphosphate (ATP) levels (Supplementary Figs. 2c and 6d) and increased lactate secretion (Supplementary Fig. 6e) in resistant cells compared to the sensitive ones. This suggests, in line with the increased glucose uptake (Fig. 2h), an increased glycolytic flux. Although glycolysis continues to use NAD^+ at the level of glyceraldehyde-3-phosphate-dehydrogenase, our $^{13}C_6$-glucose tracer experiments showed that resistant cells diverted glucose-derived carbons into glycerol-3-phosphate at a higher rate compared to the sensitives ones (Supplementary Fig. 6f, g), thus regenerating NAD^+ from NADH. In addition, analysis of a $^{13}C_5$-glutamine labeling experiment showed that resistant cells increased reductive carboxylation (Supplementary Fig. 6c, h) as a result of the increased α-ketoglutarate to citrate ratio dictated by the lower NAD^+ availability (Supplementary Fig. 6i), as reported for cancer cells with impaired mitochondrial activity[33]. It has been recently shown that polyunsaturated fatty acid desaturation is another possible mechanism used by eukaryotic cells to recycle glycolytic NAD^+[34]. In support of our hypothesis, we found that resistant cells had increased levels of highly unsaturated fatty acid (Supplementary Fig. 6j), compared to the sensitive ones. Of note, fatty acid elongation is also a source of $NADP^+$ and we observed an increase in fatty acid chain length in resistant cells (Supplementary Fig. 6j).

To validate our hypothesis that resistant cells may restrain serine synthesis due to the need of maintaining NAD^+ availability, we modulated NAD^+ levels in our resistant cells. Supplementation with α-ketobutyrate (αKB), an electron acceptor that is converted by lactate dehydrogenase to α-hydroxybutyrate thus regenerating NAD^+ but not contributing carbons to downstream pathways (Fig. 5e)[35], rescued the proliferation of resistant cells under serine/glycine deprivation and carboplatin treatment (Fig. 5f). These data show that increasing NAD^+/NADH ratio (Fig. 5g) to a certain threshold, by increasing NAD^+ levels and to a less extent NADH levels (Supplementary Fig. 6k, l), can be enough to overcome the stress induced by carboplatin treatment under serine/glycine deprivation in resistant cells. Importantly, αKB supplementation also led to re-expression of PHGDH (Fig. 5h), suggesting that NAD^+ availability is a constraint for PHGDH activity in our resistant cells.

Together, the metabolic adaptations observed in resistant cells, schematically illustrated in Fig. 5d, support a scenario in which sensitive cells would funnel most of the glucose into biosynthetic pathways to support their requirements of high proliferation rates. Once exposed to platinum and adapted to grow under its pressure, however, cells switch their central carbon metabolism toward what we speculate could be a NAD^+-regenerating phenotype, by reducing NAD^+-using activities such as serine biosynthesis.

Since our findings point to NAD^+ metabolism as one of the players in adaptations to platinum exposure, we hypothesized that resistant cells could also be susceptible to NAD^+-depleting strategies. Although both sensitive and resistant cells responded to the Nicotinamide Phosphoribosyltransferase (NAMPT) inhibitor FK866 (APO866, Daporinad) due to the lack of de novo NAD^+ synthesis[36,37], we found that resistant cells were two times more sensitive to FK866 compared to the sensitive cells, with a GI50 of 0.65 and 1.41 nM, respectively (Fig. 5i). Interestingly, while low-dose treatment with 0.4 nM FK866 as single agent had only a minor effect, in combination with carboplatin it strongly impaired proliferation of resistant cells (Fig. 5j). Moreover, RNA-seq data showed that resistant cells underwent a major reshuffling in NAD^+-dependent dehydrogenases and other NAD^+-related enzymes compared to sensitive cells (Supplementary Fig. 7a). In addition, carboplatin treatment altered the expression of these enzymes in sensitive cells, but not in the resistant ones (Supplementary Fig. 7a).

Taken together, our data suggest that resistant cells with downregulated serine biosynthesis also show global metabolic rearrangement toward a NAD^+-sparing phenotype, and that pharmacological NAD^+-depleting agents, such as NAMPT inhibitors, may be potentially combined with platinum to overcome resistance.

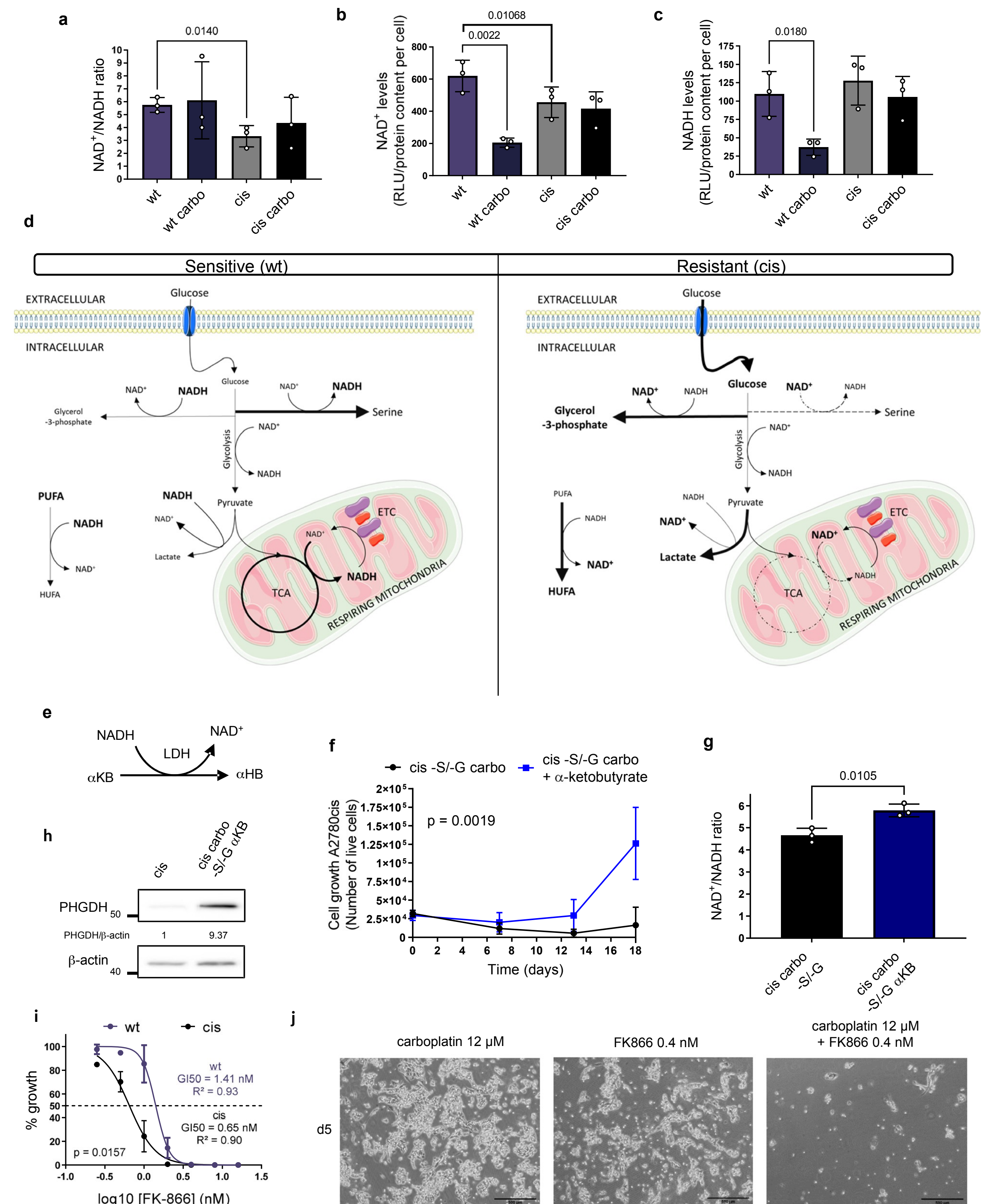

Resistant cells with decreased serine biosynthetic activity sustain PARP activity under platinum treatment

Because in resistant cells we observed a NAD$^+$-sparing phenotype but not a net increase in NAD$^+$ levels, we hypothesized that resistant cells would reshuffle their NAD$^+$-related metabolism to counteract for excessive NAD$^+$-consumption. PARPs are major NAD$^+$-consuming enzymes involved in DNA repair in eukaryotic cells [38], and A2780 resistant cells are known to have higher ability to tolerate and repair platinum-induced DNA damage, compared to wt cells [39]. A phenotype we confirmed by γH2AX staining and by showing their normal cell cycle profile under treatment (Supplementary Fig 7b, c). Since we observed that resistant cells actively regenerate NAD$^+$ but do not increase their NAD$^+$ levels compared to the sensitive ones, we hypothesized that they may consume more NAD$^+$ through PARP activation

Fig. 5 | Resistant cells rewire NAD^+-regenerating pathways. NAD^+/NADH ratio (a), NAD^+ levels b and NADH levels (c) determined by NAD^+/NADH-Glo bioluminescent Promega assay, n = 3 biological replicates (with three technical replicates each time), unpaired two-tailed t-tests, data are represented as mean ± SD. d Metabolic map and observed alterations of wt vs. cis cells, more elaborate results in Supplementary Fig. 6. e The use of α-ketobutyrate (αKB) by lactate dehydrogenase (LDH) to generate α-hydroxybutyrate (αHB) and NAD^+. f 2 mM αKB supplementation of serine/glycine starved cis cells with 6 µM carboplatin treatment, n = 3 biological replicates (with three technical replicates each time), repeated measures two-way ANOVA, data are represented as mean ± SD, p = 0.0019. g NAD^+/NADH ratio of αKB supplemented serine/glycine starved cis cells with carbo treatment, n = 3 biological replicates (with three technical replicates each time), unpaired two-tailed t-test, data are represented as mean ± SD, p = 0.0105. h Representative western blot of PHGDH in αKB supplemented carboplatin treated ser/gly starved cis cells, n = 3 biological replicates. i GI50 of wt and cis cells to the NAMPT inhibitor Daporinad determined with trypan blue counting, n = 4 biological replicates (with three technical replicates each), unpaired two-tailed t-test between GI50 values, data are represented as mean ± SEM, p = 0.0157. j Representative images of cis cells under 12 µM carboplatin and 0.4 nM Daporinad treatment and its combination, scale bar is 500 µm, n = 3 biological replicates (with three technical replicates each). Some schematic art pieces in d were used and modified from Servier Medical Art. Servier Medical Art by Servier is licensed under a Creative Commons Attribution 3.0 Unported License (https://creativecommons.org/licenses/by/3.0/). Source data are provided as a Source Data file. Carbo carboplatin treated, αKB α-ketobutyrate, αHB α-hydroxybutyrate, LDH lactate dehydrogenase, ETC electron transport chain, TCA trycarboxylic acid cycle, PUFA polyunsaturated fatty acids, HUFA highly unsaturated fatty acids.

and thus we measured levels and activity of PARP1, the most abundant member of the PARP family involved in DNA damage. We observed that resistant cells expressed higher PARP1 levels compared to the sensitive ones (Fig. 6a), and showed evidence of sustained PARP activity, measured as histone PARylation capacity, under carboplatin treatment (Fig. 6b). Interestingly, we observed a significantly decrease in PARylation in resistant cells overexpressing PHGDH (Fig. 6c), and that our serine synthesis-reactivated cis SSP cells decreased PARP1 expression again, while increasing PHGDH levels and carboplatin sensitivity (Figs. 3a, b, e and 6d). This suggests that in our resistant cells PHGDH and PARP could compete for NAD^+ availability. In line, using ovarian cancer cell line data from the Cancer Cell Line Encyclopedia (CCLE) and Genomics of Drug Sensitivity Consortium (GDSC)[40], we found that PHGDH-low expressing ovarian cancer cell lines were more resistant to the PARP inhibitor olaparib (Fig. 6e). We then investigated the effect of pharmacological PARP inhibition in resistant cells exposed to acute platinum treatment. While resistant cells had a higher GI50 value for the PARP inhibitor olaparib compared to sensitive cells (Fig. 6f), likely due to the observed higher PARP activity (Fig. 6a, b), we observed an additive effect of the PARP inhibitors in combination with carboplatin in decreasing the proliferation of resistant cells (Fig. 6g, h). We then tested the same combination treatment strategy in an additional in vitro model, the OVCAR3 cell line, originally derived from ovarian cancer ascites isolated from a HGSC patient refractory to cisplatin, cyclophosphamide and Adriamycin treatment, also commonly used to investigate platinum resistance[41]. Although in vitro we observed a higher sensitivity to carboplatin compared to the A2780 resistant cells (Supplementary Fig. 7d), we confirmed also in OVCAR3 that combination of sub-lethal doses of carboplatin and olaparib impaired growth and induced cell death (Fig. 6i). Of note, olaparib as monotherapy had limited effect on both cell lines, confirming our hypothesis that sustaining PARP activity may play a role in survival of resistant cells specifically under carboplatin pressure.

We also tested the possibility of combining olaparib and FK866 on resistant A2780cis cells and OVCAR3 cells, and we found that the combination can indeed slow down cell growth in both cell lines, however the effect was milder compared to the carboplatin-olaparib combination (Supplementary Fig. 7e, f).

Taken together, our data show that the observed NAD^+-regenerating phenotype in resistant cells is associated with sustained PARP activity and sustains cell survival upon acute platinum treatment.

PARP inhibition re-sensitizes organoids derived from resistant PDX models to carboplatin

Since low serine biosynthetic activity and increased dependence on exogenous serine seemed to be peculiar vulnerabilities of platinum-resistant tumors also in vivo, we tested the susceptibility of two additional HGSC cancer PDX models named OVC4 and OVC5 to PARP inhibition combined with carboplatin, using PDX-derived organoid cultures (Fig. 7a–d). OVC4 has been established from a patient who developed resistance several years after diagnosis while the OVC5 model has been established from a mucinous ovarian cancer patient with an acquired resistant tumor (Supplementary Table 3). First we analyzed both organoid models by H&E staining and PAX8 and mutant p53 IHC, and we matched with corresponding PDX models (Supplementary Fig. 8a, b). OVC5 organoid cultures were more resistant to carboplatin than OVC4 cultures as shown by their GI50 values (16.10 µM vs. 7.59 µM and 4.12 µM, respectively, Supplementary Fig. 8c). The treatment experiment on both organoid cultures confirmed our findings in the cell lines, with the combination significantly affecting cancer growth and almost no effect for any of the single treatments (Fig. 7a–d). These data validate our in vitro findings in clinically relevant ex vivo samples, and suggest that at least a fraction of resistant tumors might be re-sensitized to platinum treatment by inhibiting their PARP dependent activity.

Since the use of PARP inhibitors is currently indicated for platinum sensitive relapses, and as maintenance after platinum for platinum sensitive patients with homologous recombination (HR) deficient tumors, we checked the mutational status of several HR-related genes in our different models. To do this, we performed whole exome sequencing (WES) on the A2780wt/cis and OVCAR3 cell lines. For all three cell lines we found a very low total mutational burden and only limited mutations in HR genes (Supplementary Fig. 8d). The same analysis for all PDX models and their derived organoids showed higher variability in total mutational burden and HR-related mutations (Supplementary Fig. 8e, f), suggesting that our findings about the potential to combine carboplatin with PARPi is independent of HR status of the different models. This could be explained by the fact that different tumors might rely on different PARP activities, spanning from DNA damage response to transcriptional regulation.

Discussion

Development of resistance to platinum-based chemotherapy is a major hurdle in the treatment of ovarian cancer and a prominent cause of its poor prognosis. While elevated serine synthesis is linked to high proliferation rates, aggressiveness and ultimately poor prognosis in different tumors[12,23,25,42], a recent report showed that its inhibition leads to increased cisplatin resistance in gastric cancer cells in vitro[43]. However, the functional and clinical relevance of serine synthesis downregulation in platinum resistance remains elusive, as well as its potential clinical exploitability. Here we show that serine biosynthesis downregulation is one of the major adaptations that a fraction of resistant cells can use to preserve intracellular NAD^+ levels, in line with the recent report that NAD^+ and NADH abundances are major constraints for serine synthesis in different cancer cell types[32,44]. The compelling hypothesis that PHGDH and PARP1 could compete for NAD^+ availability under platinum-induced stress is not surprising in light of the recent discovery that under metabolic stress the concomitant presence of both enzymes in the nucleus can create local NAD^+ gradients, thus influencing PARP-mediated transcriptional activities[45].

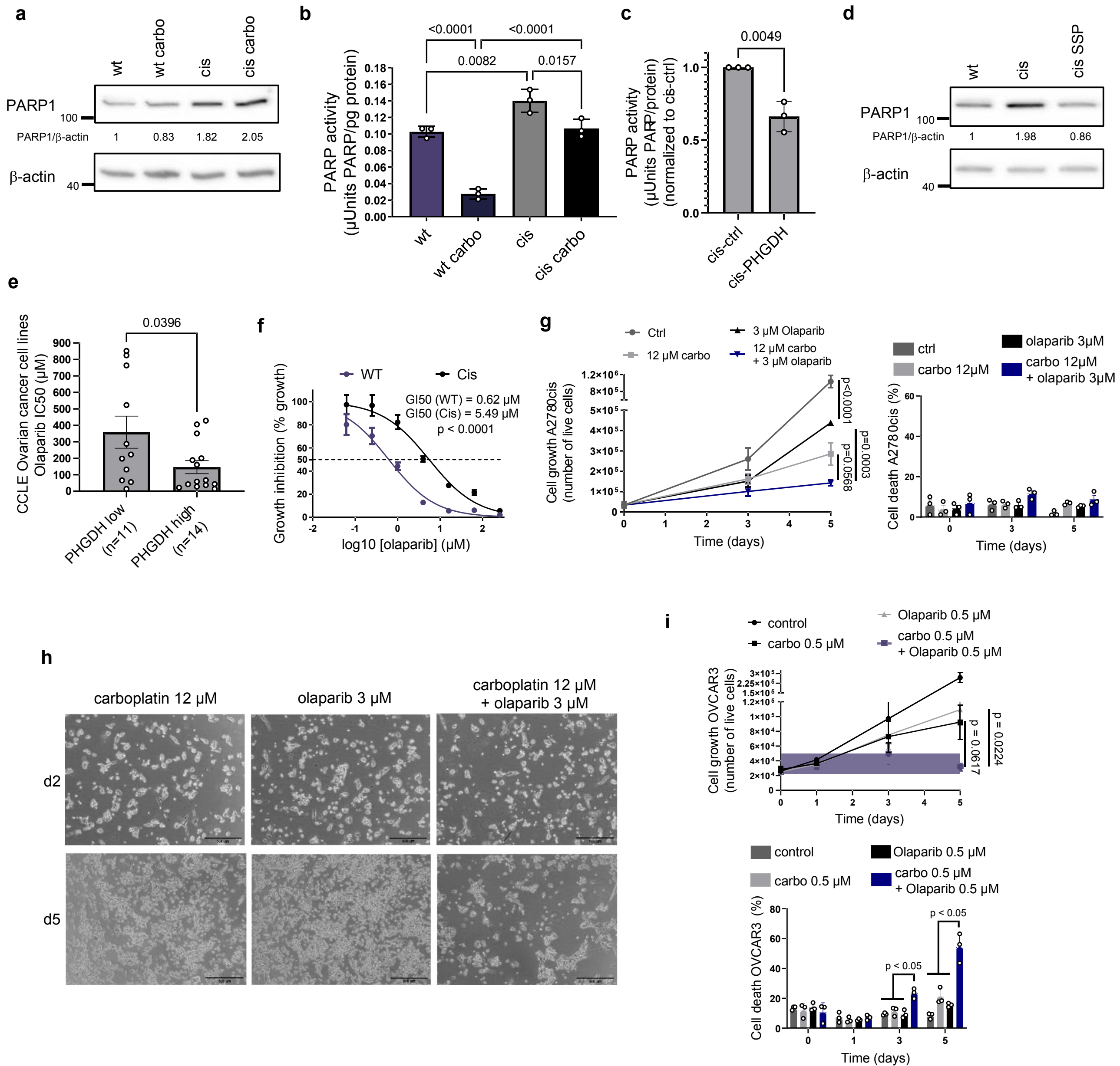

Fig. 6 | Resistant cells with decreased serine synthesis sustain PARP activity under carboplatin treatment. a Western blot of PARP1 in wt and cis cells, n = 4 biological replicates. PARP activity in carboplatin treated wt and cis cells (b) and in cis-PHGDH overexpressing cells (c), n = 3 biological replicates (with three technical replicates each), ordinary one-way ANOVA with Tukey's multiple comparison post-test, data are represented as mean ± SD with $p < 0.0001$ (b) and n = 3 biological replicates (with three technical replicates each), unpaired two-tailed t-test, data are represented as mean ± SD, $p = 0.0049$ c. d Western blot of PARP1 in cis SSP cells, n = 2 biological replicates. e Olaparib sensitivity of PHGDH ^{low} and PHGDH^{high} expressing ovarian cancer cell lines, data obtained from the CCLE (gene expression) and GDSC (drug sensitivity), n = 25 divided in PHGDH^{low} (PHGDH mRNA Z < 0, n = 11) and PHGDH^{high} (PHGDH mRNA Z > 0, n = 14) subgroups, unpaired two-tailed t-test, error bars represent SEM, $p = 0.0396$. f GI50 value of wt and cis cells for the PARP inhibitor olaparib, n = 3 biological replicates (with three technical replicates each), unpaired two-tailed t-test between GI50 values, data are represented as mean ± SD, $p < 0.0001$. Growth and cell death of cis cells with 12 μM carboplatin and 3 μM olaparib and its combination, n = 3 biological replicates (with 2–3 technical replicates each) (left panel is a representative figure with n = 2 technical replicates), two-way ANOVA with Tukey's multiple comparison post-test at day 5, data are represented as mean ± SEM with $p < 0.0001$ (g) and its representative images, scale bar is 500 μm, n = 3 h. i Growth (left) and cell death (right) of OVCAR3 cells under 0.5 μM carboplatin and 0.5 μM olaparib and its combination, n = 3 biological replicates (with three technical replicates each), unpaired two-tailed t-test at day 5 with $p = 0.0617$ and $p = 0.0224$ for carbo + olaparib vs carbo or olaparib, respectively (left) and two-way ANOVA with Tukey's multiple comparison post-test with $p = 0.0424$ (right), data are represented as mean ± SEM. Source data are provided as a Source Data file. Carbo carboplatin treated, CCLE Cancer Cell Line Encyclopedia, GDSC Genomics of Drug Sensitivity in Cancer.

However, serine biosynthetic activity and serine dependency have never been associated with platinum response in ovarian cancer before. Our data in PDX models and the analysis of matched clinical samples collected at diagnosis and at relapse also show that this phenotype may be acquired gradually in a subset of patients, due to subsequent exposure to platinum-based therapy cycles. This is particularly relevant, since most of the patients experience several response-relapse-response events during the course of their disease. Although further studies comparing matched biopsies prospectively and longitudinally collected from larger series of patients are needed to validate these findings, our results suggest that serine biosynthetic activity, and specifically PHGDH and intratumor serine levels, could

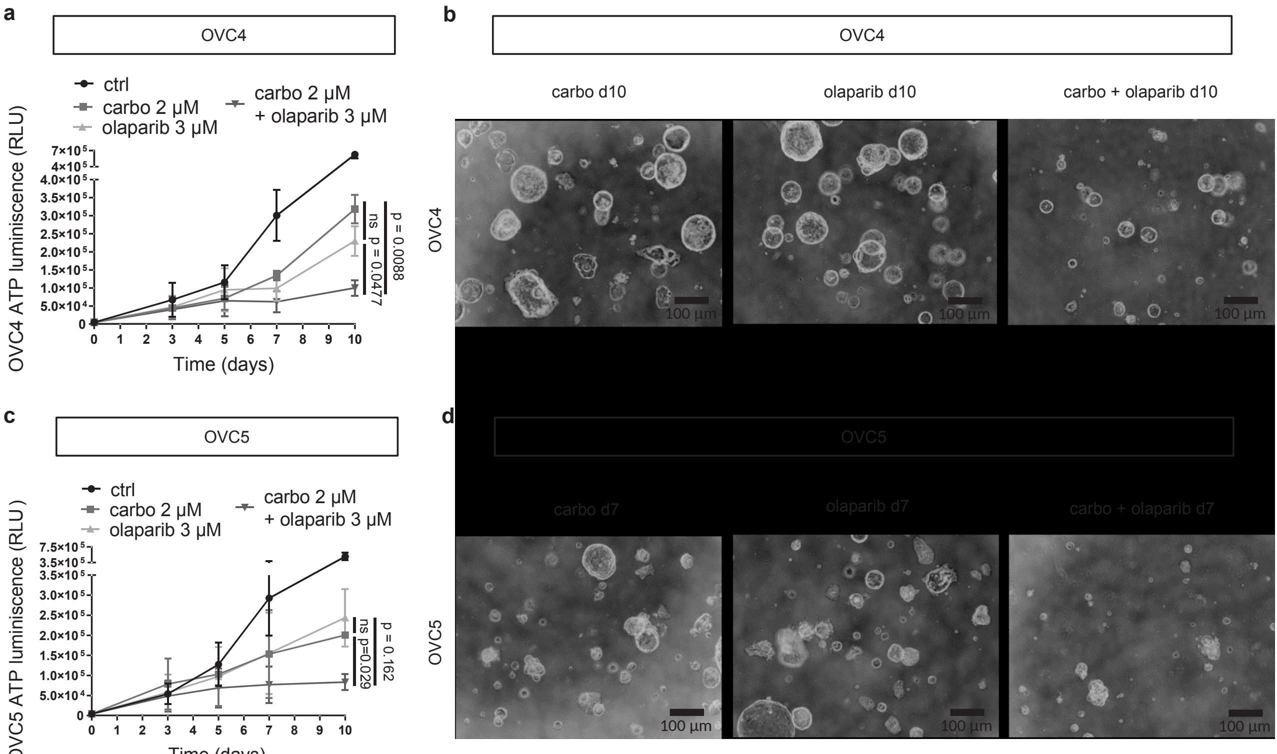

Fig. 7 | PARPi re-sensitizes resistant PDX-derived organoids to carboplatin. Growth of a OVC4 organoids under carboplatin and olaparib single agent treatment and its combination, determined by adenosine triphosphate (ATP) measurement, n = 3 biological replicates (with six technical replicates each), data are represented as mean ± SEM, unpaired two-tailed t-test performed at day 10, and b its representative pictures, scale bar is 100 µm. Growth of c OVC5 organoids under carboplatin and olaparib single agent treatment and its combination, determined by ATP measurement, n = 2 biological replicates for treatment groups and n = 3 for ctrl growth (with six technical replicates each), data are represented as mean ± SEM, unpaired two-tailed t-test performed at day 10, and d its representative pictures, scale bar is 100 µm. Source data are provided as a Source Data file. Carbo carboplatin treated organoids.

potentially predict development of platinum resistance in a subgroup of patients.

Our findings have twofold implications, shedding light on mechanisms underlying the multiple adaptions described so far for different pathways involved in glucose, glutamine and amino acids metabolism in platinum-resistant ovarian cancers, but also revealing unexpected vulnerabilities that can potentially be exploited to re-sensitize resistant cells [19,46]. Specifically, our data suggest that both PARP and NAD^+ biosynthesis inhibition, in combination with platinum-based chemotherapy, could be considered for patients with resistant disease that decrease serine biosynthesis. The original approval of three different PARP inhibitors (olaparib, niraparib and rucaparib) as maintenance therapy for recurrent platinum sensitive patients with gBRCA mutations marked an important advance in the management of ovarian cancer patients[47–49]. Clinical evidence shows that also patients without BRCA mutation or homologous recombination deficiency (HRD) could benefit from PARP inhibitors and this might not be limited to the maintenance setting [48,50]. Intriguingly, mutational analysis of our preclinical models suggests that response to carboplatin-olaparib combination in resistant patients seem to be HRD-independent. However, a systematic definition of the HR status in research subjects is needed to be able to draw firm conclusions, highlighting the importance of future prospective studies in HR status-defined patients sampled longitudinally after platinum treatments. In this view and considering the low expected response rate to other chemotherapies in resistant patients (10–15%), the possibility to at least temporarily control the progression of tumors by combining platinum and PARP inhibitors is appealing. In addition, since in the imminent future PARP inhibitors will be used also in earlier clinical settings and patients will be exposed to such drugs for longer periods, the adoption of NAD^+ synthesis inhibitors could potentially overcome development of acquired resistance to PARPi. Further proof-of-concept studies are needed to clinically validate our preliminary findings. While open questions remain, not the least if our findings and the metabolic vulnerabilities we uncovered are specific for ovarian cancer, our data provide a rationale for future studies to assess the relation between serine biosynthesis and platinum resistance in ovarian cancer and additional tumor types treated with platinum-based chemotherapy.

Methods

Cell culture

A2780wt and its cisplatin resistant analog A2780cis cells were obtained from the ECACC (Sigma-Aldrich ECACC 93112519 and Sigma-Aldrich ECACC 93112517, respectively) and were maintained in RPMI medium containing 10% FBS (Gibco), 2 mM glutamine (L-Glutamine, Gibco), 100 IU penicillin and 100 µg/ml streptomycin (PenStrep, Gibco). OVCAR3 cell line was purchased from the ATCC (NIH:OVCAR-3 (ATCC® HTB-161™)) and were also grown in RPMI medium containing 10% FBS, glutamine and PenStrep. They were authenticated using short tandem repeat profiling. HEK293T cells were obtained from ATCC (CRL-3216™) and were grown in DMEM containing 10% FBS (Gibco), 2 mM glutamine (L-Glutamine, Gibco), 100 IU penicillin and 100 µg/ml streptomycin (PenStrep, Gibco). Cell lines were routinely tested for Mycoplasma contamination and they were generally used for experiments between passages 10 and 25.

Chemotherapeutic agents and chemicals

Carboplatin was provided by the university hospital Leuven (UZL), who purchased it from Hospira. NAC, αKB, FK866 (Daporinad), L-$^{13}C_5$-glutamine and L-$^{13}C_3$-serine were obtained from Sigma-Aldrich, whereas

D-glucose $^{13}C_6$ was purchased from Cambridge Isotope Laboratories. Olaparib (AZD2281) was purchased from Selleckchem. All ingredients to make fresh RPMI were purchased from Sigma-Aldrich. Hygromycin B was purchased from Invitrogen, G418 sulfate (Geneticin) and puromycin were purchased from Gibco.

Antibodies
PHGDH (HPA021241, 1:2000 for western blot, 1:4000 or 1:8000 for IHC for the Norwegian and Dutch cohort, respectively) and PSPH (HPA020376, 1:1000 for western blot) antibodies were purchased from Sigma-Aldrich. The PSAT1 (CPTC-PSAT1-2, 1:500 for western blot) and PARP1 (AFFN-PARP1-17B10, 1:150 for western blot) antibodies, developed by the National Cancer Institute and EMBL MACF, respectively, were obtained from the Developmental Studies Hybridoma Bank, created by the NICHD of the NIH and maintained at The University of Iowa, Department of Biology, Iowa City, IA 52242. The phospho-Histone H2A.X (Ser139) (20E3, 1: 600 for IF), ATF4 (D4B8, 1:1000 for WESTERN BLOT) and β-actin (13E5, 1:5000, for western blot) antibodies were purchased from Cell Signaling Technology. Anti-p53 Antibody [DO-1]-Chip graded was obtained from Abcam (ab1101, 1:200 for IHC) while PAX8 Polyclonal antibody was obtained from Proteintech (10336-1-AP, 1:1200 for IHC). Secondary peroxidase conjugated goat anti-rabbit (111-035-003, 1:5000 for western blot (1:10 000 for β-actin western blot)) and goat anti-mouse antibodies (115-035-044, 1:10,000 for western blot) were purchased from Jackson ImmunoResearch. Secondary donkey anti-rabbit Alexa Fluor 594 (1:800) was purchased from Molecular Probes, Life Technologies.

Cell growth and death assay
Cell proliferation and death were analyzed by counting total cell number with a hemocytometer after staining with trypan blue. Medium was changed on day 0 and 2 and every other 3 days after. Cell numbers were determined at time points indicated in figures. All experiments were performed at day 5, except if stated otherwise. For experiments under serine/glycine deprivation conditions, cells were fed homemade medium (homemade RPMI with the same formulation as commercial RPMI from Gibco, supplemented with 10% dialyzed FBS (Gibco) and standard concentrations of penicillin-streptomycin and glutamine) with or without serine and/or glycine (Sigma-Aldrich).

Genetic overexpression of catalytically-active PHGDH and catalytic-dead PHGDH (CD-PHGDH)
Overexpression of PHGDH was performed as described before [26]. The overexpression of PHGDH in A2780cis cells was performed using the pLHCX plasmid expressing the PHGDH cDNA obtained from the lab of S.M.F. The empty plasmid pLHCX was used as a control. Retroviral particles were produced using the pCL Ampho retroviral packaging plasmid in HEK293T cells. Infection of A2780cis cells was performed overnight (ON) with freshly prepared virus and the medium was replaced the next day. Cells were selected with hygromycin (400 µg/ml for initial selection, 200 µg/ml as maintenance concentration). Lentiviral overexpression of CD-PHGDH was performed using pCW plasmid expressing codon optimized catalytically inactive PHGDH (D175N, R236K, H283A). pCW-codon optimized catalytically inactive PHGDH was a gift from Michael Pacold (Addgene plasmid # 154903; RRID:Addgene_154903)[31]. The empty pCW57-MCS1-P2A-MCS2 (Neo) plasmid was used as control. pCW57-MCS1-P2A-MCS2 (Neo) was a gift from Adam Karpf (Addgene plasmid # 89180; RRID:Addgene_89180). Lentiviral particles were produced using the pCMV delta R8.91 and pCMV-VSV-G plasmids (packaging and envelope plasmids, respectively) in HEK293T cells. Infection of A2780cis cells was performed ON with freshly prepared virus and the medium was replaced the next day. Cells were selected with Geneticin (800 µg/ml for initial selection, 500 µg/ml as maintenance concentration). Overexpression of (CD-) PHGDH was validated by western blot analysis.

Knock-down of PHGDH
PHGDH was knocked-down in platinum sensitive cells using two commercially available shRNAs targeting PHGDH (TRCN0000255351 and TRCN0000233029), using MISSION shRNA lentiviral transduction particles (Sigma). Mission pLKO.1-puro Non-target shRNA control transduction particles (SHC016V-1EA, Sigma) were used as control. In total, 150,000 cells were seeded per well in a 12-well plate. The next day, the lentivirus was put on the cells with a MOI of 0.5 in the presence of 5 µg/ml polybrene. After 24 h, medium was replaced with pre-warmed complete growth medium. On day 3, infected cells were selected and further grown in the presence of 2 µg/ml puromycin (Gibco).

Microscopy
For light microscopy, pictures were taken with a Leica DFC295 (for cells) or Leica DM5500 (for tissue) microscope and Leica Application Suite Version 3.7.0 or LAS AF imaging software, respectively (Leica Microsystems CMS GmBH). Immunofluorescence images were acquired with a fluorescence Olympus BX41 microscope with XC30 camera and X-cite series 120 Q lamps. Using cellSens Dimension software. Analysis of microscopic pictures was done using ImageJ.

Immunofluorescence
Cells were fixed with 4% formaldehyde for 15 min. Next, specimens were blocked with 10% normal donkey serum (Sigma)/0.3% Triton X-100 in 1X PBS (Gibco) for 1 h and incubated ON at 4 °C with primary antibody. Afterwards cells were incubated for 45 min in the dark with donkey anti-rabbit Alexa Fluor 594. Finally, slides were mounted with Prolong Gold antifade reagent with DAPI (Molecular Probes P36935, Thermo Fisher) and visualized with fluorescence microscopy.

Cell cycle analysis
Cell cycle phases were analyzed using dual Click-iT EdU Alexa Fluor 488 and FxCycle Violet staining (Molecular Probes, Life Technologies) according to the manufacturer's protocol and analyzed using flow cytometry (BD FACSCanto II, BD Biosciences).

Oxygen consumption
OCR was determined using a Seahorse XF24 Extracellular flux analyzer (Seahorse Bioscience). In total, 150,000 cells per well were seeded in a XF24 Cell Culture Microplate (Seahorse Bioscience) 24 h before the measurements. OCR was measured under basal conditions and after injection with oligomycin, FCCP and antimycin A, as described before[52].

Western blot
Cells were lysed in Pierce RIPA Buffer (Thermo Fisher) supplemented with phosphatase and protease inhibitors (Roche-04906845001, Roche-04698116001). Protein concentrations were determined using Pierce BCA Protein Assay Kit (Thermo Fisher) and detected with a Multiskan spectrophotometer (Thermo Fisher). In total, 20 µg of protein was loaded in each lane, except in Fig. 4h where 6 and 36 µg protein were loaded for OVC1a and OVC2, respectively, due to the inherent different nature of the tumors. Before running, protein sample was reduced in reducing buffer (50 mM DTT, 2x Laemmli sample buffer (BioRad)) and heated at 95 °C for 5 min and then separated on a 10-well Mini-PROTEAN TGX Precast Any-KD gel (BioRad) for 10 min at 100 V and subsequent ~40–50 min at 160 V. Gels were blotted onto a Mini Trans-Blot nitrocellulose membrane (BioRad) using 300 mA for 1 h, according to manufacturer's protocol. The membrane was stained with 0.1% Ponceau-Xyline in 5% acetic acid (Sigma) for 1 min to visualize blotted protein bands on the membrane. Membrane was cut into pieces when needed, using the Spectra™ Multicolor Broad Range Protein Ladder (Thermo) as reference. After washing, the membrane was blocked for 1 h at room temperature in 10% fat-free milk in TBS-T

buffer, incubated with primary antibodies with appropriate dilution (see "antibodies") at 4 °C ON and subsequently with secondary antibody for 1 h at room temperature. Bands were visualized using SuperSignal West Dura Extended Duration Substrate (Thermo Fisher) and images were captured using an Azure c600 detection system (Azure Biosystems). Densitometric quantification was performed using ImageJ.

ATP, and NAD^+ and NADH level determination

ATP was measured using ATP-lite assay, NAD^+ and NADH levels and ration were determined using NAD^+/NADH-glo assay. All assays were purchased from Promega and experiments were executed according to manufacturer's protocol. Bioluminescence was measured with Victor X4 plate reader (PerkinElmer).

PARP activity assay

PARP activity was determined as PARylation levels in cell extracts on a histone coated 96-well plate. It was measured using the HT Colorimetric PARP/Apoptosis Assay (Trevigen) and experiments were executed according to manufacturer's protocol. Absorbance was detected with a Multiskan spectrophotometer (Thermo Fisher).

Oxidative stress detection

Mitochondrial superoxide production was detected by measuring MitoSOX (Thermo Fisher, M36008) fluorescence while CellROX Deep Red Reagent (Thermo Fisher, C10422r) was used to measure total cellular ROS with flow cytometry (BD FACSCanto II, BD Biosciences), according to manufacturer's protocol.

H&E staining

Four µm thick FFPE slides were deparaffinized with toluol (2 × 5 min) and ethanol (2 × 5 min). Slides were incubated in haematolylin solution (Gill3, Prosan) for 4 min. Afterwards slides were dipped three times in 1% HCl in technical ethanol and dipped three times in saturated Li_2CO_3 solution. Slides were stained for 3 min using eosine and dehydratation was done using propanol (3 times 3 dips) and xylol (3 times 3 dips). Between different steps, slides were washed with tap water and deionized water, respectively. Finally, slides were covered using Depex and covered glass.

P53 and PAX8 IHC

PAX8 and p53 IHC on organoid FFPE slides were done by routine IHC procedure. In brief, slides were dewaxed in xylene (PAX8)/toluol (p53) and rehydrated in graded ethanol solution. Endogenous peroxidase activity was blocked by 0.3% H_2O_2 in methanol solution for 30 min. Heat-induced epitope retrieval was done using sodium citrate buffer (10 mM, pH = 6) at 95 °C for 30 min (PAX8) or 1 h (p53). Slides were cooled down to room temperature for 20 min, after which they were blocked for 1 h at room temperature in blocking buffer (2% BSA, 1% dry milk, 0,10% Tween20) + 10% goat serum (for PAX8). Next, sections were incubated overnight at RT (PAX8) or 4 °C (p53) with primary antibody in a humid chamber. Primary antibodies were diluted as described in "Antibodies" in blocking buffer + 1% goat serum (for PAX8). The following day slides were incubated and detected using Envision+/HRP mouse reagent (K400111-2, Agilent) for 30 min for p53. PAX8 slides were incubated with HRP-conjugated secondary antibody for 30 min at room temperature. Visualization was done by applying DAB as chromogenic substrate. Finally, slides were dehydrated in ethanol followed by xylene and sections were mounted with a cover slide using DPX.

Isotope tracer experiments and GC-LC/MS analysis

Cells were seeded in 6-well plates at a density of 50,000 cells per well in complete medium for proliferation and metabolite assays (day −1). The following day, cells were grown in medium with or without 6 µM carboplatin. At day 2, medium was aspirated, cells washed with PBS, and fresh glucose- or glutamine free RPMI (Gibco) supplemented with $^{13}C_6$-glucose (CLM-1396-5, Cambridge Isotope Laboratories, Inc.) or $^{13}C_5$-L-glutamine (605166, Sigma-Aldrich), respectively, 10% dialyzed FBS, 2 mM glutamine, 100 IU penicillin, 100 µg/ml streptomycin, with or without 6 µM carboplatin, was added. At day 5, cells were washed with 0.9% NaCl, and quenched by placing the plate in liquid nitrogen and stored at −80 °C. Alternatively, quenching and metabolite extraction was also performed after 24 h.

Metabolite extraction and detection by gas chromatography/mass spectrometry or liquid chromatography/mass spectrometry was performed as described before[26,53]. Metabolites were extracted with 800 µl of $MeOH/H_20$ (5:3) (v:v) containing 0.6 µg/ml of glutaric acid on a dry ice/ice mixture, scraped, transferred to 2-ml tube, vortexed (10 min, 4 °C) and centrifuged (10 min, 20,000 × g, 4 °C). The supernatants were dried ON under vacuum at 4 °C.

Gas chromatography/mass spectrometry (GC/MS). Samples were derivatized using methoxyamine hydrochloride and N-methyl-N-tert-butyldimethylsilyltrifluoroacetamide (TBDMS). Samples were dissolved in 20 µl of 20 mg/ml methoxyamine hydrochloride in pyridine (MOX) (Pierce) at 37 °C for 90 min. Samples were centrifuged for 5 min, and 7.5 µl of supernatant was transferred to a glass vial. Samples were then derivatized by adding 15 µl TBDMS + 1% tert-butyldimethylchlorosilane (TBDMCS; Pierce) for 1 h at 60 °C. Analysis was performed on an Agilent 7890A GC system coupled to an Agilent 5975C Inert MS system with an electron impact ionization set at 70 eV operating in SIM mode. Metabolites were separated with a DB35MS column (30 m, 0.25 mm, 0.25 µm) using helium carrier gas at a flow rate of 1 ml/min. A volume of 1 µl of sample were injected with a split ratio 1 to 3 with an injector set at 270 °C. For metabolite separation, the GC oven temperature was set at 100 °C for 1 min ramped to 105 °C at 2.5 °C/min, then to 240 °C at 3.5 °C/min and finally to 320 °C at 22 °C/min. Data were collected by Masshunter version 10.1 build 10.1.48 (Agilent). Fractional enrichment of ^{13}C in metabolites was corrected for the natural abundance using an in-house script written in Matlab using the method developed by Fernandez et al.[54] Metabolites abundances were also normalized to the internal standard glutaric acid.

Liquid chromatography/mass spectrometry (LC/MS). For the detection of metabolites by LC-MS, a Dionex UltiMate 3000 LC System (Thermo Scientific) with a thermal autosampler set at 4 °C, coupled to a Q Exactive Orbitrap mass spectrometer (Thermo Scientific) was used. Samples were resuspended in 50 µl of water and a volume of 10 µl of sample was injected on a C18 column (Acquity UPLC HSS T3 1.8 µm 2.1 × 100 mm).The separation of metabolites was achieved at 40 °C with a flow rate of 0.25 ml/min. A gradient was applied for 40 min (solvent A: 10 mM Tributyl-Amine, 15 mM acetic acid—solvent B: Methanol) to separate the targeted metabolites (0 min: 0% B, 2 min: 0% B, 7 min: 37% B, 14 min: 41% B, 26 min: 100% B, 30 min: 100% B, 31 min: 0% B; 40 min: 0% B). The MS operated in negative full scan mode (m/z range: 70–1050 and 300–700 from 5 to 25 min) using a spray voltage of 4.9 kV, capillary temperature of 320 °C, sheath gas at 50.0, auxiliary gas at 10.0. Data were collected using the Xcalibur software v4.0 (Thermo Scientific) and analyzed with Matlab for the correction of protein content and natural abundance, but also to determine the isotopomer distribution using the method developed by Fernandez et al.[54].

Lipid profiling

Cells were collected at day 5 and dissolved in 800 µl DPBS. In total, 100 µl of the suspension was used for protein determination using the BCA assay (Thermo Fisher). The remaining suspension was used for lipid extraction as described before[55]. Samples were homogenized in 0.9 ml 1 N HCl/CH3OH ULC/MS (1:8, v/v) (Biosolve), 0.8 ml CHCl3

(Sigma-Aldrich) and 200 µg/ml of the antioxidant 2,6-di-tert-butyl-4-methylphenol (BHT, Sigma). The suspension was shaken for 10 min and spun (SS-34, 12,000 rpm for 5 min at 4 °C with the brake ON). The lower phase was collected to glass tubes and evaporated under vacuum (Speed Trap, Thermo Fisher) for 30 min at room temperature. Samples were sparged with Argon (Sigma) and stored at −20 °C. At the day of analysis, the samples were reconstituted in CH3OH/CHCl3/NH4OH (72:8:1, v/v/v) and lipid standards were added (Avanti Polar Lipids). Phospholipids were analyzed by electrospray ionization tandem mass spectrometry (ESI-MS/MS) with a hybrid quadrupole linear ion trap mass spectrometer (4000 QTRAP system, AB SCIEX) equipped with a TriVersa NanoMate robotic nanosource (Advion Biosciences). The collision energy was varied as follows: prec 184, 50 eV; nl 141, 35 eV; nl 87, −40 eV; prec 241, −55 eV. The system was operated in the multiple reaction monitoring mode for quantification of individual species. Typically, a 3-min period of signal averaging was used for each spectrum.

RNA-seq analysis

In total, 5×10^6 cells per condition per replicate were lysed using RLT buffer (Qiagen) and stored at −80 °C. RNA-seq was performed using HiSeq2500 platform (Illumina) (SR-65bp) at the Genomics Core facility of the NKI-AvL (Amsterdam, the Netherlands). Raw RNA-seq FASTQ files were aligned with STAR to the human genome GRCh37.p13. The file formats were then converted using SAMtools. Reads were counted at exons of protein-coding genes using HTSeq with gencode.v19 annotation. Normalization of library size for the read counts and differential expression analysis was performed using DEseq and DEseq2 with standard parameters. RNA-seq data have been deposited into the NCBI Gene Expression Omnibus database (http://www.ncbi.nlm.nih.gov/geo/) under accession number GSE176218.

Whole exome sequencing (WES)

Genomic DNA of cells, organoids and tumors was extracted using the DNeasy Blood & Tissue kit (Qiagen) according to the manufacturer's protocol. WES was performed at the UZ Leuven Genomics Core. For WES, libraries were made on Sciclone (PerkinElmer, USA) using KAPA HyperPrep kit (Roche, WI, USA) and IDT Dual Indexed Adapters (IDT, USA). Exons were enriched through hybridization with a custom version of the in-solution Twist Biosciences Human Comprehensive Exome kit. The enriched libraries were then amplified and sequenced on NovaSeq 6000 as Paired end 150 bp (Illumina, CA, USA). WES were processed using an in-house pipeline. Base-calling was performed with bcl2fastq (version 2.19.0). Reads were aligned to the human reference genome GRCh38 using BWA mem (version 0.7.17), duplicate reads were marked using Picard MarkDuplicates (version 2.22.1) and base quality scores were recalibrated using GATK BaseRecalibrator and ApplyBQSR (version 4.1.7). Finally, single nucleotide variants and small indes were called using GATK HaplotypeCaller (version 4.1.7) and annotated using Annovar (version 2019Oct24). Variant filtering was performed in R based on quality score, coverage and pathogenicity score. Variants with a Phred corrected quality score of <50, a coverage of <10x and >243 and Phred corrected CADD pathogenicity score <15 were removed. Variants that met these requirements were incorporated into the final mutation annotation format and further processed with the R package maftools for visualization. The WES data generated in this study have been deposited in the SRA database under accession code PRJNA816435.

PDX studies

The establishment of patient-derived xenografts has been approved by the Commission of Medical Ethics of the University Hospitals Leuven (S54185; ML8713) and by the KU Leuven EC (P038/2015) and informed consent from the patients was obtained for PDX establishment. In vivo work was done at the TRACE PDX platform (KU Leuven), according to the ARRIVE guidelines. To establish the PDX models, tumor fragments freshly isolated from patients were implanted in the inter-scapular fat pad of female immunodeficient nude mice (NMRI-Fox1nu strain, Taconic). Mice were housed in groups of 5 in filter top cages and maintained in a semi-SPF facility at 22 °C (±2 °C) with 14 h light/10 h dark cycle and humidity between 45–70%. Bedding was replaced once a week. Mice were 5–10 weeks old at the moment of tumor implantation. Tumors were propagated in at least three generations of mice and characterized by histologic and SNP-analysis to confirm genealogy before conducting experiments on cohorts of "xenopatients".

For each treatment experiment, 25–50 mice were implanted with tumors in order to obtain enough material and statistical significance. Tumors were grown until a volume of ~300–400 mm^3 was reached and were then included in treatment. Four days before actual treatment, mice were put on control diet (Baker Amino Acid Diet 5CC7, TestDiet) or serine/glycine-free diet (Mod TestDiet 5CC7 w/No Added Serine or Glycine 5BJX, TestDiet). Tumor biopsies were taken before the start of treatment. For implantation and biopsies, mice were anesthetized with 75 mg/kg ketamine (Anesketin) and 100 mg/kg medetomidine (Narcostart) intraperitoneal injection, biopsies were taken with disposable biopsy punch needles (2.5 mm, Kai Medical), postoperative care was given by 0.05 mg/kg Buprenorphine (Vetergisic) subcutaneous and reversal of anesthesia was done by Atipamezole (Antisedan) 1 mg/kg subcutaneous.

As treatment, placebo (0.9% saline) or carboplatin (50 mg/kg) was injected intraperitoneal (IP) once a week for 3 weeks. During treatment, tumor size was monitored twice a week by measuring its length (L) and width (W) with a caliper and the volume (V) was estimated by $V = L \times W^2 \times \pi/6$. One week after the last treatment, mice were euthanized if there was still tumor tissue present. Whenever the tumor disappeared by the end of the treatment, mice were saved and monitored for relapse. At the time of relapse, mice were treated again with carboplatin. According to the KU Leuven Ethics Committee approved protocol for our experiments (P038/2015), mice were euthanized whenever tumors reached a volume of more than 2000 mm^3. This limit has been exceeded for the serine/glycine-free diet experiment with OVC2 because the model grew fast, being extremely vascularized and prone to develop liquid cysts. These data were however needed to evaluate the effect of the used diets. At any time, we monitored potential discomfort of the mice as also reported in the Ethics Committee approved document, and mice were euthanized in case any of the specified limits was reached. At euthanasia, mice were anesthetized and euthanized by cervical dislocation and blood was collected using cardiac punction. Samples were taken for protein and metabolite analysis. Proteins were extracted in Pierce RIPA Buffer (Thermo Fisher) using Lysing matrix A tubes (MP Bio) and the Precellys 24 (Bertin technologies) for lysis. Metabolites were extracted using a cryomill (Retsch) under liquid nitrogen conditions and samples were further processed as described before.

Organoid isolation and treatment

For organoid derivation, the method described in Kopper et al. was adopted[56]. Briefly, surgical mouse tumor specimens were cut into small pieces followed by digestion with Ad-DF+++ (Advanced DMEM/F12 (Gibco) containing 1x Glutamax (Gibco), 10 mM HEPES (Gibco) and antibiotics) supplemented with 1.5 mg/ml Collagenase II (Sigma), 10 µg/ml Hyalurondiase type IV-S (Sigma), 500x primocin (InvivoGen) and 1000x Y-27632 (Rho/Rock pathway inhibitor) and incubated on an orbital shaker for 1 h at 37 °C. Suspension was strained over a 100 µm filter. After centrifugation, red blood cells were lysed in 2 ml red cell lysis buffer for 5 min at room temperature followed by additional wash steps with Ad-DF+++ medium. Next, cells were suspended in a 2:1 ratio in cold Ad-DF+++ medium:Geltrex basement membrane matrix (Gibco) and, after plating, let to solidify upside down.

Finally, ovarian cancer organoid cell growth medium with appropriate growth factors as described by Kopper et al.[56] was added. Treatment experiments were done as described by Ooft et al.[57]. Briefly, organoid cultures were dissociated using TrypLE (Gibco) for 10 min at 37 °C, filtered and replated to grow for 4 days in order to obtain uniform sized, usable organoids. Next, cultures were collected and incubated for 15 min with dispase II (Roche) to remove Geltrex, organoids were counted and seeded in clear-bottom, white-walled 96-well plates (Corning Incorporated) in 1:2 AD-DF+++:Geltrex at a concentration of 20 organoids/µl, 5 µl per well. After solidification, drugs were added in the Ad-DF+++ medium (200 µl/well). Readouts were obtained at day 0 and 5 and quantification of cell viability was done using CellTiter-Glo 3D (Promega), according to manufacturer's protocol, read using a Victor X4 Plate Reader (PerkinElmer). Pictures were taken by light microscopy. Organoids were characterized by performing H&E analysis on FFPE blocks.

Effusion specimens and immunohistochemistry (IHC) of the Norwegian cohort

Effusions consisted of 18 HGSC specimens (16 peritoneal, 2 pleural) submitted to the Department of Pathology at the Norwegian Radium Hospital during the period of 1999 to 2008. Effusion specimens were diagnosed by an experienced cytopathologist (B.D.) based on morphology in smears and cell blocks, prepared using the thrombin clot protocol, and IHC, based on established guidelines. Informed consent was obtained according to national and institutional guidelines. Study approval was given by the Regional Committee for Medical Research Ethics in Norway (S-04300).

Formalin-fixed, paraffin-embedded sections from the 18 effusions were analyzed for PHGDH protein expression using the Dako EnVision Flex + System (K8012; Dako, Glostrup, Denmark). The PHGDH antibody was a rabbit polyclonal antibody purchased from Sigma (Prestige Antibodies, powered by Atlas Antibodies; cat # HPA021241; Stockholm, Sweden), applied at a 1:4000 dilution following antigen retrieval in Low pH buffer (pH 6.0).

Following deparaffinization and antigen retrieval, sections were treated with EnVision™ Flex + mouse linker (15 min) and EnVision™ Flex/HRP enzyme (30 min) and stained for 10 min with 3'3-diaminobenzidine tetrahydrochloride (DAB), counterstained with hematoxylin, dehydrated and mounted in Toluene-Free Mounting Medium (Dako). Positive control consisted of normal pancreas.

IHC scoring. Staining was scored by an experienced cytopathologist (B.D.), using a 0–4 scale for staining extent as follows: 0 = no staining, 1 = 1–5%,2 = 6–25%,3 = 26–75%,4 = 76–100% of tumor cells. Staining intensity was scored as 0, 1 or 2, corresponding to negative, weak or strong staining. Values were combined by doubling, providing a 0–8 score.

The only patient with PHGDH increase at recurrence was aged between 60 and 65 years. Both mean and median age of the PHGDH equal subgroup was 50 years with SD of 12 years. The mean age of the PHGDH decreasing subgroup was 67 years, while the median age was 68 years, SD for this subgroup was 10 years.

Tumor specimen and immunohistochemistry (IHC) of the Dutch cohort

Patients with HGSC FIGO stage IIb-IV, treated with cytoreductive surgery and adjuvant chemotherapy (PDS) or neoadjuvant chemotherapy followed by interval debulking surgery in the tertiary referral hospital The Netherlands Cancer Institute—Antoni van Leeuwenhoek Hospital (NKI-AVL) between January 2008 and December 2015 were selected. Recurrence data of the aforementioned patients who were treated in the NKI-AVL were retrieved from patient files. Last check of patient files took place on October 31, 2020. Patients from whom recurrence tissue was extracted, either via biopsy or during surgery, in the NKI-AVL were included. For the present study, approval of the institutional review boards of the Netherlands Cancer Registry (NCR, K19.074), Dutch Pathology Registry (PALGA, 2019-169) and NKI-AVL (CFMPB297) was obtained. The requested dataset was considered anonymous and the use is therefore exempt from ethics review board approval according to Dutch legislation.

Formalin-fixed, paraffin-embedded (FFPE) tissue blocks from both the primary tumor and the recurrence samples were obtained. Diagnosis of the primary tumor was confirmed based on conventional morphological examination of sections stained with hematoxylin and eosin (H&E) by an expert pathologist (H.M.H.). The paraffin tissue blocks of the primary tumor were organized into TMAs. Representative areas for immune cell scoring of the tumor center and the peripheral invasive margin were selected on whole-tissue FFPE H&E stained slides. In each tumor four cores were selected, optimally representing tumor and peripheral stroma. TMAs with 1 mm sized cores were constructed, using a tissue microarrayer (Grand Master, Sysmex Europe GmbH, Norderstedt, Germany). To enable adhesion of the cores to the recipient paraffin block, the block was melted at 70 °C for 9 min and cooled down ON. In case of the recurrence samples, whole slides were used as samples were not large enough to obtain multiple TMA's. IHC was performed on the BenchMark Ultra autostainer (Ventana Medical Systems Inc., USA). Three µm thick TMA sections were generated and heated at 75 °C for 28 min followed by deparaffinization and rehydration. Deparaffinization was completed in the instrument using EZ prep solution (Ventana Medical Systems Inc., USA). Heat-induced antigen retrieval was initiated using Cell Conditioning 1 (Ventana Medical Systems Inc., USA) for 64 min at 95 °C. PHGDH was detected using a polyclonal antibody (cat: HPA021241) (1/8000 dilution, 64 min at 36 °C, Sigma-Aldrich). Bound antibody was detected using the OptiView DAB Detection Kit (Ventana Medical Systems). Slides were counterstained with Hematoxylin II and Bluing Reagent (Ventana Medical Systems).

IHC scoring. The IHC staining results of PHGDH were scored by an expert pathologist (H.M.H.) semiquantitatively by integrating intensity and distribution. Intensity was divided into categories of 0, no staining; 1, weak staining; 2, moderate staining and 3, strong staining. Staining distribution was based on the percentage of positive tumor cells (0–100%). The final PHGDH expression score was obtained by multiplying the intensity- and distribution-scores, with 0 corresponding to no staining and 300 to 100% of cells with 3+ staining intensity.

The mean and median age of the PHGDH increasing subgroup is 62 and 63 years, respectively, with a SD of 9 years. Both mean and median age of the PHGDH equal subgroup was 74 years with SD of 4 years. Both mean and median age of the PHGDH decreasing subgroup was 63 years, with a SD of 10 years.

CCLE–TCGA data analysis

Computational data from The Cancer Genome Atlas[27] were accessed and processed using cBioPortal (http://www.cbioportal.org/)[58,59] and Microsoft Office Excel, respectively. Drug sensitivity data from the CCLE were accessed using the Genomics of Drug Sensitivity in Cancer (GDSC) database (https://www.cancerrxgene.org/)[40] and linked with gene expression data using cBioPortal.

Data processing and statistics

Data processing was done in Microsoft Office Excel 2019; ImageJ, Microsoft Office Excel and PowerPoint 2019 was used for microscopy and western blot processing; FlowJo 10 was used for flow cytometry analysis; Matlab was used for metabolomics analysis; additional specialized softwares were used as described in the specific "Method" sections and the "Reporting summary". Figures were generated using GraphPad Prism 9. Statistical analysis was done using the available GraphPad Prism 9 tools. Each experiment was performed at least three

times as biological replicates with at least three technical replicates each time, except if stated otherwise in the figure legends. Data are represented as mean ± standard deviation or standard error. Significance was evaluated using the statistical tests and post-tests as described in the figure legends. p Values are indicated in the figures. For GI50 determination in GraphPad Prism, drug concentrations were log10 transformed and subsequently the non-linear regression built in three parameter log(inhibitor) vs. response function was used. The top constraint was put at 100, while the bottom constraint was set at 0, no constraint was set to the Hill slope.

Reporting summary

Further information on research design is available in the Nature Research Reporting Summary linked to this article.

Data availability

The RNA-seq data generated in this study have been deposited in the GEO database under accession code GSE176218. The WES data generated in this study have been deposited in the SRA database under accession code PRJNA816435.The used metabolomics data and the raw metabolomics data can be found in the source data file. Data from the TCGA were obtained using cBioPortal: https://www.cbioportal.org/ (Ovarian Cystadenocarincoma, TCGA, Nature 2011). Gene expression data from the CCLE were obtained using cBioPortal: https://www.cbioportal.org/ (Cancer Cell Line Encyclopedia, Broad 2019). Drug sensitivity data were obtained from the GDSC, using https://www.cancerrxgene.org/ (STUDY: olaparib, Pubchem 23725625, sample size 762, screening site Sanger, dataset GDSC2). Source data are provided with this paper.

References

1. Vasan, N., Baselga, J. & Hyman, D. M. A view on drug resistance in cancer. Nature 575, 299–309 (2019).
2. Sung, H. et al. Global Cancer Statistics 2020: GLOBOCAN estimates of incidence and mortality worldwide for 36 cancers in 185 countries. CA Cancer J. Clin. 71, 209–249 (2021).
3. Lheureux, S., Braunstein, M. & Oza, A. M. Epithelial ovarian cancer: evolution of management in the era of precision medicine. CA Cancer J. Clin. 69, 280–304 (2019).
4. Patch, A. M. et al. Whole-genome characterization of chemoresistant ovarian cancer. Nature 521, 489–494 (2015).
5. Lheureux, S., Gourley, C., Vergote, I. & Oza, A. M. Epithelial ovarian cancer. Lancet 393, 1240–1253 (2019).
6. Pujade-Lauraine, E., Banerjee, S. & Pignata, S. Management of platinum-resistant, relapsed epithelial ovarian cancer and new drug perspectives. J. Clin. Oncol. 37, 2437–2448 (2019).
7. Binju, M. et al. Mechanisms underlying acquired platinum resistance in high grade serous ovarian cancer—a mini review. Biochim. Biophys. Acta. Gen. Subj. 1863, 371–378 (2019).
8. Hanahan, D. Hallmarks of cancer: new dimensions. Cancer Disco. 12, 31–46 (2022).
9. Vander Heiden, M. G. & DeBerardinis, R. J. Understanding the intersections between metabolism and cancer biology. Cell 168, 657–669 (2017).
10. Potter, M., Newport, E. & Morten, K. J. The Warburg effect: 80 years on. Biochem. Soc. Trans. 44, 1499–1505 (2016).
11. Wise, D. R. & Thompson, C. B. Glutamine addiction: a new therapeutic target in cancer. Trends Biochem. Sci. 35, 427–433 (2010).
12. Locasale, J. W. et al. Phosphoglycerate dehydrogenase diverts glycolytic flux and contributes to oncogenesis. Nat. Genet. 43, 869–874 (2011).
13. Green, D. R., Galluzzi, L. & Kroemer, G. Cell biology. Metabolic control of cell death. Science 345, 1250256 (2014).
14. Kanarek, N. et al. Histidine catabolism is a major determinant of methotrexate sensitivity. Nature 559, 632–636 (2018).
15. Komurov, K. et al. The glucose-deprivation network counteracts lapatinib-induced toxicity in resistant ErbB2-positive breast cancer cells. Mol. Syst. Biol. 8, 596 (2012).
16. Pommier, A. J. et al. Leptin, BMI, and a metabolic gene expression signature associated with clinical outcome to VEGF inhibition in colorectal cancer. Cell Metab. 23, 77–93 (2016).
17. Zaal, E. A. & Berkers, C. R. The influence of metabolism on drug response in cancer. Front Oncol. 8, 500 (2018).
18. Gentric, G. et al. PML-regulated mitochondrial metabolism enhances chemosensitivity in human ovarian cancers. Cell Metab. 29, 156–173.e110 (2019).
19. Obrist, F. et al. Metabolic vulnerability of cisplatin-resistant cancers. EMBO J. 37 https://doi.org/10.15252/embj.201798597 (2018).
20. Fendt, S. M., Frezza, C. & Erez, A. Targeting metabolic plasticity and flexibility dynamics for cancer therapy. Cancer Disco. 10, 1797–1807 (2020).
21. Possemato, R. et al. Functional genomics reveal that the serine synthesis pathway is essential in breast cancer. Nature 476, 346–350 (2011).
22. Sullivan, M. R. et al. Increased serine synthesis provides an advantage for tumors arising in tissues where serine levels are limiting. Cell Metab. 29, 1410–1421.e1414 (2019).
23. Yang, M. & Vousden, K. H. Serine and one-carbon metabolism in cancer. Nat. Rev. Cancer 16, 650–662 (2016).
24. Zhang, B. et al. PHGDH defines a metabolic subtype in lung adenocarcinomas with poor prognosis. Cell Rep. 19, 2289–2303 (2017).
25. Rinaldi, G. et al. In vivo evidence for serine biosynthesis-defined sensitivity of lung metastasis, but not of primary breast tumors, to mTORC1 inhibition. Mol. Cell 81, 386–397.e387 (2021).
26. Rossi, M. et al. PHGDH heterogeneity potentiates cancer cell dissemination and metastasis. Nature https://doi.org/10.1038/s41586-022-04758-2 (2022).
27. TCGA. Integrated genomic analyses of ovarian carcinoma. Nature 474, 609–615 (2011).
28. Behrens, B. C. et al. Characterization of a cis-diamminedichloroplatinum(II)-resistant human ovarian cancer cell line and its use in evaluation of platinum analogues. Cancer Res. 47, 414–418 (1987).
29. Labuschagne, C. F., van den Broek, N. J., Mackay, G. M., Vousden, K. H. & Maddocks, O. D. Serine, but not glycine, supports one-carbon metabolism and proliferation of cancer cells. Cell Rep. 7, 1248–1258 (2014).
30. Ye, J. et al. Pyruvate kinase M2 promotes de novo serine synthesis to sustain mTORC1 activity and cell proliferation. Proc. Natl Acad. Sci. USA 109, 6904–6909 (2012).
31. Maddocks, O. D. et al. Serine starvation induces stress and p53-dependent metabolic remodelling in cancer cells. Nature 493, 542–546 (2013).
32. Diehl, F. F., Lewis, C. A., Fiske, B. P. & Vander Heiden, M. G. Cellular redox state constrains serine synthesis and nucleotide production to impact cell proliferation. Nat. Metab. 1, 861–867 (2019).
33. Gaude, E. et al. NADH shuttling couples cytosolic reductive carboxylation of glutamine with glycolysis in cells with mitochondrial dysfunction. Mol. Cell 69, 581–593.e587 (2018).
34. Kim, W. et al. Polyunsaturated fatty acid desaturation is a mechanism for glycolytic NAD. Cell Metab. 29, 856–870.e857 (2019).
35. Sullivan, L. B. et al. Supporting aspartate biosynthesis is an essential function of respiration in proliferating cells. Cell 162, 552–563 (2015).
36. Tolstikov, V., Nikolayev, A., Dong, S., Zhao, G. & Kuo, M. S. Metabolomics analysis of metabolic effects of nicotinamide phosphoribosyltransferase (NAMPT) inhibition on human cancer cells. PLoS ONE 9, e114019 (2014).

37. Tan, B. et al. Pharmacological inhibition of nicotinamide phosphoribosyltransferase (NAMPT), an enzyme essential for NAD+ biosynthesis, in human cancer cells: metabolic basis and potential clinical implications. J. Biol. Chem. 288, 3500–3511 (2013).
38. Bai, P. Biology of Poly(ADP-Ribose) polymerases: the factotums of cell maintenance. Mol. Cell 58, 947–958 (2015).
39. Masuda, H. et al. Increased DNA repair as a mechanism of acquired resistance to cis-diamminedichloroplatinum (II) in human ovarian cancer cell lines. Cancer Res. 48, 5713–5716 (1988).
40. Yang, W. et al. Genomics of Drug Sensitivity in Cancer (GDSC): a resource for therapeutic biomarker discovery in cancer cells. Nucleic Acids Res. 41, D955–D961 (2013).
41. Hamilton, T. C. et al. Characterization of a human ovarian carcinoma cell line (NIH:OVCAR-3) with androgen and estrogen receptors. Cancer Res. 43, 5379–5389 (1983).
42. Mattaini, K. R. et al. Increased PHGDH expression promotes aberrant melanin accumulation. BMC Cancer 19, 723 (2019).
43. Zhao, X., Fu, J., Tang, W., Yu, L. & Xu, W. Inhibition of serine metabolism promotes resistance to cisplatin in gastric cancer. Onco Targets Ther. 13, 4833–4842 (2020).
44. Murphy, J. P. et al. The NAD^+ salvage pathway supports PHGDH-driven serine biosynthesis. Cell Rep. 24, 2381–2391.e2385 (2018).
45. Ma, C. et al. The alternative activity of nuclear PHGDH contributes to tumour growth under nutrient stress. Nat. Metab. 3, 1357–1371 (2021).
46. Ricci, F. et al. Overcoming platinum-acquired resistance in ovarian cancer patient-derived xenografts. Ther. Adv. Med. Oncol. 11, 1758835919839543 (2019).
47. Moore, K. et al. Maintenance olaparib in patients with newly diagnosed advanced ovarian cancer. N. Engl. J. Med. 379, 2495–2505 (2018).
48. González-Martín, A. et al. Niraparib in patients with newly diagnosed advanced ovarian cancer. N. Engl. J. Med. 381, 2391–2402 (2019).
49. Coleman, R. L. et al. Rucaparib maintenance treatment for recurrent ovarian carcinoma after response to platinum therapy (ARIEL3): a randomised, double-blind, placebo-controlled, phase 3 trial. Lancet 390, 1949–1961 (2017).
50. Oza, A. M. et al. Olaparib combined with chemotherapy for recurrent platinum-sensitive ovarian cancer: a randomised phase 2 trial. Lancet Oncol. 16, 87–97 (2015).
51. Ngo, B. et al. Limited environmental serine and glycine confer brain metastasis sensitivity to PHGDH inhibition. Cancer Disco. 10, 1352–1373 (2020).
52. Eelen, G. et al. Role of glutamine synthetase in angiogenesis beyond glutamine synthesis. Nature 561, 63–69 (2018).
53. Elia, I. et al. Proline metabolism supports metastasis formation and could be inhibited to selectively target metastasizing cancer cells. Nat. Commun. 8, 15267 (2017).
54. Fernandez, C. A., Des Rosiers, C., Previs, S. F., David, F. & Brunengraber, H. Correction of 13C mass isotopomer distributions for natural stable isotope abundance. J. Mass Spectrom. 31, 255–262 (1996).
55. Talebi, A. et al. Sustained SREBP-1-dependent lipogenesis as a key mediator of resistance to BRAF-targeted therapy. Nat. Commun. 9, 2500 (2018).
56. Kopper, O. et al. An organoid platform for ovarian cancer captures intra- and interpatient heterogeneity. Nat. Med. 25, 838–849 (2019).
57. Ooft, S. N. et al. Patient-derived organoids can predict response to chemotherapy in metastatic colorectal cancer patients. Sci. Transl. Med. 11 https://doi.org/10.1126/scitranslmed.aay2574 (2019).
58. Cerami, E. et al. The cBio cancer genomics portal: an open platform for exploring multidimensional cancer genomics data. Cancer Disco. 2, 401–404 (2012).
59. Gao, J. et al. Integrative analysis of complex cancer genomics and clinical profiles using the cBioPortal. Sci. Signal 6, pl1 (2013).
60. Ihlenfeldt, W. D., Bolton, E. E. & Bryant, S. H. The PubChem chemical structure sketcher. J. Cheminform 1, 20 (2009).

Acknowledgements

We are grateful to all past and present members of the Amant, Fendt and Agami laboratories for invaluable discussions and advice, and acknowledge the technical help of Tina Everaert and Rossana Maria Benedetto. We thank Mr. Arild Holth for the IHC staining of the effusion samples of the Norwegian cohort. We would like to acknowledge the NKI-AVL Core Facility Molecular Pathology & Biobanking (CFMPB) for supplying NKI-AVL Biobank material and lab support, for the staining of the Dutch cohort samples. We also thank TRACE, the KU Leuven PDX Platform, for technical assistance with the in vivo experiments. We would like to thank Jonas Dehairs and Frank Vanderhoydonc of the KU Leuven lipidomics core facility Lipometrix for performing lipidomics analysis. Finally, we would like to thank the Genomics Core Facilities of the Netherlands Cancer Institute and the UZ Leuven for RNA-seq analysis and WES analysis, respectively. Some schematic art pieces in Fig. 5d and Supplementary Fig. 2d were used and modified from Servier Medical Art (http://smart.servier.com/). Servier Medical Art by Servier is licensed under a Creative Commons Attribution 3.0 Unported License (https://creativecommons.org/licenses/by/3.0/). Chemical structures in Supplementary Fig. 3h are generated using PubChem Sketcher[60]. This study was supported by research grants from Kom Op Tegen Kanker—The Flemish Cancer Society (3M150511, to F.A., S.M.F. and D.L.) and KWF Kanker Bestrijding (11574, to R.A., F.A. and D.A.). F.A. is a senior researcher for Research Foundation—Flanders (FWO). T.V.N. is recipient of an Emmanuel van der Schueren fellowship from Kom op Tegen Kanker—The Flemish Cancer Society. M.R. has received consecutive postdoctoral fellowships from FWO and Stichting tegen Kanker, and J.A.G.D. was supported by FWO. S.M.F. acknowledges funding from the European Research Council under the ERC Consolidator Grant Agreement n. 771486–MetaRegulation, FWO—Research Projects (G088318N), KU Leuven FTBO, Fonds Baillet Latour, King Baudouin Foundation and the Beug Foundation. TRACE staff is supported by Stichting Tegen Kanker grant 2016-054. P.C. is supported by Grants from Methusalem funding (Flemish government), the Fund for Scientific Research-Flanders (FWO-Vlaanderen), ERC Advanced Research Grant EU-(ERC743074), and a NNF Laureate Research Grant from Novo Nordisk Foundation (Denmark).

Author contributions

Conceptualization: T.V.N., J.A.G.D., L.V.W., H.M.H., E.A.Z., C.R.B., R.A., S.M.F., D.A. and F.A.; Methodology: T.V.N., M.P., J.A.G.D., L.V.W., H.M.H., W.D.W., D.A., M.R., E.A.Z., C.R.B., A.T., J.V.S, B.D. and S.M.F.; Investigation: T.V.N., M.P., L.V.W., J.A.G.D., R.E.M.B.A., M.R., H.M.H., S.M., A.T., G.E., E.A.Z., B.D., P.R.K. and D.A.; Resources: H.M.H., L.R., E.B., G.S.S., P.C., J.V.S., C.R.B., B.D., S.M.F., R.A., F.A.; Writing—original draft: T.V.N. and D.A.; Visualization: T.V.N.; Supervision: S.M.F., D.A. and F.A.; Funding acquisition: T.V.N., R.A., D.L., S.M.F., D.A. and F.A.

Competing interests

S.M.F. has received funding from Bayer, Merck and BlackBelt Therapeutics and has consulted for Fund+. G.S.S. reports institutional research support from AstraZeneca, Merck, Novartis, and Roche, unrelated to this work. All the other authors declare no competing interests.

https://doi.org/10.1038/s41467-022-32272-6

Additional information

Supplementary information The online version contains supplementary material available at https://doi.org/10.1038/s41467-022-32272-6.

Correspondence and requests for materials should be addressed to Daniela Annibali or Frédéric Amant.

Peer review information Nature Communications thanks Clare Scott and the other, anonymous, reviewer(s) for their contribution to the peer review of this work. Peer reviewer reports are available.

Reprints and permission information is available at http://www.nature.com/reprints

Publisher's note Springer Nature remains neutral with regard to jurisdictional claims in published maps and institutional affiliations.

Open Access This article is licensed under a Creative Commons Attribution 4.0 International License, which permits use, sharing, adaptation, distribution and reproduction in any medium or format, as long as you give appropriate credit to the original author(s) and the source, provide a link to the Creative Commons license, and indicate if changes were made. The images or other third party material in this article are included in the article's Creative Commons license, unless indicated otherwise in a credit line to the material. If material is not included in the article's Creative Commons license and your intended use is not permitted by statutory regulation or exceeds the permitted use, you will need to obtain permission directly from the copyright holder. To view a copy of this license, visit http://creativecommons.org/licenses/by/4.0/.

© The Author(s) 2022

[1]Gynecological Oncology Laboratory, Department of Oncology, KU Leuven and Leuven Cancer Institute (LKI), 3000 Leuven, Belgium. [2]Division of Oncogenomics, Oncode Institute, The Netherlands Cancer Institute, 1066 CX Amsterdam, The Netherlands. [3]Laboratory of Cellular Metabolism and Metabolic Regulation, VIB-KU Leuven Center for Cancer Biology, VIB, Herestraat 49, 3000 Leuven, Belgium. [4]Laboratory of Cellular Metabolism and Metabolic Regulation, Department of Oncology, KU Leuven and Leuven Cancer Institute (LKI), Herestraat 49, 3000 Leuven, Belgium. [5]Department of Obstetrics and Gynecology, Maastricht University Medical Centre, Maastricht, The Netherlands. [6]GROW, School for Oncology and Developmental Biology, Maastricht, The Netherlands. [7]Department of Research, Netherlands Comprehensive Cancer Organization (IKNL), Utrecht, The Netherlands. [8]Biomolecular Mass Spectrometry and Proteomics, Bijvoet Center for Biomolecular Research, Utrecht University, 3584 CH Utrecht, The Netherlands. [9]Division of Cell Biology, Metabolism and Cancer, Department Biomolecular Health Sciences, Faculty of Veterinary Medicine, Utrecht University, 3584 CL Utrecht, The Netherlands. [10]Laboratory of Lipid Metabolism and Cancer, Department of Oncology, KU Leuven and Leuven Cancer Institute (LKI), 3000 Leuven, Belgium. [11]TRACE PDX Platform, Department of Oncology, KU Leuven and Leuven Cancer Institute (LKI), 3000 Leuven, Belgium. [12]Department of Medical Oncology, The Netherlands Cancer Institute, 1066 CX Amsterdam, The Netherlands. [13]Division of Molecular Pathology, The Netherlands Cancer Institute, 1066 CX Amsterdam, The Netherlands. [14]Laboratory of Angiogenesis and Vascular Metabolism, VIB-KU Leuven Center for Cancer Biology, VIB, Department of Oncology, KU Leuven and Leuven Cancer Institute (LKI), 3000 Leuven, Belgium. [15]Department of Development and Regeneration, KU Leuven, 3000 Leuven, Belgium. [16]Center for Biotechnology, Khalifa University of Science and Technology, Abu Dhabi, United Arab Emirates. [17]Laboratory of Angiogenesis and Vascular Heterogeneity, Department of Biomedicine, Aarhus University, 8000 Aarhus, Denmark. [18]Laboratory for Translational Genetics, Department of Human Genetics, KU Leuven, 3000 Leuven, Belgium. [19]VIB Center for Cancer Biology, VIB, 3000 Leuven, Belgium. [20]University of Oslo, Faculty of Medicine, Institute of Clinical Medicine, N-0316 Oslo, Norway. [21]Department of Pathology, Oslo University Hospital, Norwegian Radium Hospital, N-0310 Oslo, Norway. [22]Erasmus MC, Department of Genetics, Rotterdam University, 3015 GD Rotterdam, The Netherlands. [23]Department of Obstetrics and Gynecology, University Hospitals Leuven and Department of Oncology, 3000 Leuven, Belgium. [24]Centre for Gynecologic Oncology Amsterdam (CGOA), Antoni Van Leeuwenhoek-Netherlands Cancer Institute (AvL-NKI), University Medical Center (UMC), Amsterdam, The Netherlands. [25]These authors contributed equally: Daniela Annibali, Frédéric Amant. ✉e-mail: daniela.annibali@kuleuven.be; frederic.amant@uzleuven.be